Environmental Science Processes & Impacts

ROYAL SOCIETY OF CHEMISTRY

PAPER

View Article Online
View Journal | View Issue

Cite this: *Environ. Sci.: Processes Impacts*, 2025, **27**, 225

Environmental impact of an acid-forming alum shale waste rock legacy site in Norway†

Mila K. Pelkonen, *[a] Estela Reinoso-Maset, [a] Gareth T. W. Law, [b] Ole Christian Lind [a] and Lindis Skipperud [a]

Alum shale formations in Scandinavia are generally enriched in uranium (U) and, when exposed to air and water, may produce acidic rock drainage (ARD), releasing potentially harmful elements into the environment. Taraldrud is a legacy site in southeast Norway where approx. 51 000 m^3 of alum shale was deposited in the 1980s–1990s. In 2006, ARD formation became obvious after high concentrations of leachable elements and low environmental pH were measured in a nearby stream. A manmade precipitation pond and liming treatments attempt to address the environmental pollution, but the site remains non-remediated. This study aimed to evaluate the extent of contamination caused by ARD and examine environmental and human health risks caused by mobilized trace elements and radionuclides. Surface water, sediment, soil, and biota samples were collected in the area and chemically and/or radiochemically analyzed to assess the prevailing concentrations within different environmental compartments. The elemental distribution and variation patterns were studied using principal component analysis. Most of the leachable elements were present in highly mobile and bioavailable forms in the pond water, out of which Cd, Mn, Ni, and U exceeded drinking water regulations. The highest enrichment in soil and sediment was for U, which was associated with the sulfide-bearing soil fraction, Fe, Cu, Mo, and As. No changes in water quality were observed between up- and downstream from the site, indicating that the Fe and S rich phases in the pond retain the leachable elements effectively under prevailing environmental conditions. This study provides valuable insights into the risks and challenges associated with ARD and where U is the main pollutant of concern.

Received 23rd May 2024
Accepted 22nd October 2024

DOI: 10.1039/d4em00298a

rsc.li/espi

Environmental significance

Acid rock drainage is created through the oxidation of sulfide-bearing minerals upon exposure to air and water, facilitated by both natural and manmade processes. Acid rock drainage can play a crucial role in the transport and accumulation of potentially harmful elements in the environment, including naturally occurring radioactive materials. A better understanding of geochemical processes governing the release and retention of leachable elements from the rock source can provide key information for minimizing the ecological risks associated with planned, ongoing, and past activities in impacted environments. Our study of an alum shale legacy site shows that even under extremely acidic water conditions where harmful elements, such as uranium, are present in a mobile and bioavailable form, formation of secondary mineral phases can hinder their migration throughout the surrounding environment.

1. Introduction

Anthropogenic activities, such as mining and construction work, often lead to the accumulation of large volumes of crushed rock waste. Waste rock rich in sulfide-bearing minerals can become acid-generating when exposed to air and water through chemical weathering.[1] This process is known as acidic rock drainage (ARD) and occurs as a result of sulfide oxidation, generating leachates characterized by low pH and high concentrations of potentially harmful and toxic elements.[1] ARD is a natural process that is accelerated by increasing access to oxidants through increased surface area in the crushed rocks, but also through microbe–mineral interactions.[2] Therefore, ARD can become an important contributor to the transfer of potentially harmful elements from waste into the surrounding

[a]*Environmental Chemistry Section, Faculty of Environmental Sciences and Natural Resource Management, Norwegian University of Life Sciences, Aas, Norway. E-mail: mila.pelkonen@nmbu.no*

[b]*Department of Chemistry, Radiochemistry Unit, The University of Helsinki, Helsinki, Finland*

† Electronic supplementary information (ESI) available: Analytical methodology; summary and details of the collected samples (surface water, porewater, soil, sediment, alum shale, plants); certified and standard reference materials; geochemical modeling (additional aqueous equilibria, saturation indices, speciation diagrams); SR-XRPD diffractograms and phase semi-quantification; gamma spectrometry results and ICP-MS/MS spectrometry comparison; accumulation of elements from alum shale to shale porewater; water size fractionation; environmental quality standards for surface waters, soils and sediments; pH depth profiles; Kruskal–Wallis test for duplicate cores; PCA (proportions, eigenvalues, biplots); transfer factors for plants. See DOI: https://doi.org/10.1039/d4em00298a

environment and to the enrichment of elements into the different environmental compartments.[3] ARD can also lead to widespread precipitation of secondary mineral phases when the oversaturated acidic runoffs encounter different environmental conditions. The composition of the secondary minerals depends on the ARD quality together with the chemical conditions of the receiving environment. When ARD is generated from sulfide-rich rocks, the secondary minerals linked to sulfide oxidation can be divided into three groups: (1) iron oxides, oxyhydroxides, and oxyhydroxysulfates (*e.g.*, goethite, hematite, schwertmannite, and jarosite) and other amorphous iron phases; (2) hydrous iron, calcium, and aluminum metal sulfates (*e.g.*, gypsum); and, (3) other metal-rich phases with crystallinity ranging from low to amorphous (*e.g.*, basaluminite, and hydrozincite).[4] The stability of secondary minerals is affected by the prevailing pH and oxidation–reduction potential (E_h) conditions and can have an important role in controlling the mobility of leachable elements.[4]

Alum shales are Cambrian–Ordovician forms of black mudrocks that have an unusually large geographical distribution, contain high levels of silicates and organic carbon, and are often enriched in sulfides and trace elements of concern, including naturally occurring radionuclides.[5,6] Alum shales within the Scandinavian Alum Shale Formation are recognized for their enriched levels of uranium (U), and due to secular equilibrium within unweathered shale, the U progenies such as the radiotoxic radium-226 (Ra-226) can pose a significant risk to humans and the environment.[6–8] The acid-forming potential of alum shale depends on its sulfide and carbonate content,[9] consequently ARD starts to form when the carbonate content is too low to buffer the produced acidity due to sulfide oxidation.

Chemical weathering of black shales through acid generation, including the neutralization by carbonate and silicate phases, is a well-known process, and the potential environmental impact and health effects it poses have been the subject of numerous studies around the world.[10–15] In Norway, formation of ARD from alum shale has been a known issue for the construction industry in Oslo since the 1950s.[16] Black mudrocks in the Oslo region can encompass more than ten sub formations, including the Alum Shale Formation horizons 2 and 3a that extend from the Middle Cambrian to the lowest Ordovician periods. These can be 20–100 m thick, are characterized by high organic carbon, sulfide, and U content, and are known to generate large quantities of ARD when exposed to surface conditions.[17] In the past, the concerns were mainly focused on the effect of ARD on concrete, but the focus has been shifting toward the environmental impact of these alum shale materials when not properly handled and stored since intrusion of air and exchange of water have been proven to increase leaching of potentially harmful elements from the alum shale debris, even at neutral pH.[13,14]

Taraldrud is an alum shale waste rock legacy site, located southeast of Oslo, Norway. It has been estimated that approximately 51 000 m^3 of alum shale waste rocks from construction activities in the Oslo municipality were used as filling material at the Taraldrud between the 1980s and 1990s.[18] The weathering of the alum shale waste rock was first noticed in 2006 when water from a stream that runs adjacent to the deposit exhibited lower pH and higher concentrations of potentially harmful elements than those measured upstream.[18] This early survey raised concerns about public health risks since the stream is connected to a river used for drinking water collection.[19] Between 2008 and 2012, actions were hence commenced by the authorities to minimize the extent of contamination. To protect the water quality of the stream, a precipitation pond (also referred to as a sedimentation pond) was built to catch the acidic seepage waters originating from the alum shale waste rock and liming has allegedly been periodically applied to increase the pH of pond water.[18] Thereafter, circumneutral pH was measured but elevated concentrations of Fe, Mn, Ni, Al, and Zn in the stream water were still reported. In a more comprehensive survey and mapping of the area from 2017, it was estimated that the average activity concentration of U in the alum shale waste rock was 1187 Bq kg^{-1} and that over 39 000 m^2 of the surrounding area had been affected by the generated acidic leachates.[18] However, the published risk assessment for human health and spreading of contaminants (*e.g.*, Al, As, Cd, Cu, Ni, Zn, and U)[18] only included the aquatic environment (*i.e.*, it was assumed that all the acidic runoffs followed the groundwater flow in the area), and precipitation of contaminants (*e.g.*, due to environmental pH increase) was not considered.

Monitoring only the levels of potentially harmful elements present in ARD is not sufficient to generate long-term predictions of their fate in the environment; specific information on their mobility is needed. Therefore, the main objective of this study was to improve the understanding of acid-forming alum shale waste rock masses and the associated environmental impact if not managed properly. The extent of contamination caused by ARD originating from the waste rock at the Taraldrud site was determined by identifying and quantifying leachable elements in different environmental compartments, including the terrestrial environment. The governing geochemical processes for mobility and retention of contaminants from the source (alum shale) to the endpoint (drinking water) at the site were deduced based on the characterization of the source, leachability, and enrichment factors, while the environmental impact of ARD was assessed by calculating transfer factors and estimating radiation doses for non-human biota. Although the environmental impact of black shales has been previously reported in the literature, this is, to our knowledge, the first study comprehensively assessing the unique contamination fingerprint, both in aquatic and terrestrial environments, resulting from weathering of Scandinavian alum shale waste rock under natural conditions and its associated environmental and radiological risks. Moreover, studying the environmental impact of alum shale under natural conditions at this Norwegian non-remediated legacy site can provide site-specific insights applicable to sub-boreal conditions of the Nordic region.

2. Materials and methods

2.1. Site description

The Taraldrud legacy site is located at a junction of E6 highway in the Nordre Follo municipality in southeast Norway,

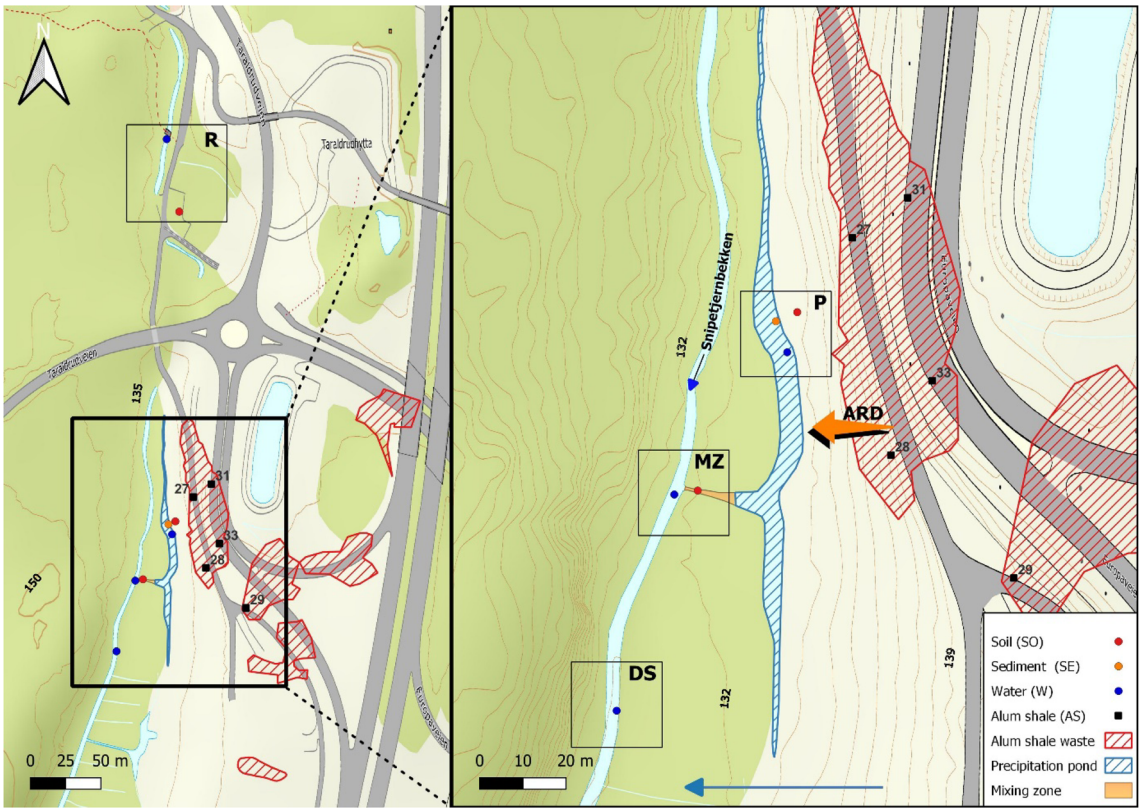

Fig. 1 Sampling locations at the Taraldrud alum shale legacy site. The orange arrow indicates the acid rock drainage (ARD) direction and the blue arrows the direction of surface and groundwater flow. The different sampling areas are marked as follows: R = reference site, P = precipitation pond, MZ = mixing zone, and DS = downstream. Color dots represent the sampling location and sample type. Dashed areas represent the location of deposited waste rock and the manmade pond, and the orange area is the connection between the pond and stream. Surface map created using QGis[20] with Kartverket[21] base map.

approximately 18 km south of Oslo. The deposited shale was used to level out rough terrain and height differences in the area and parts of the waste rock now lie under the exit ramp of the E6 highway.[18] The deposit is located next to a natural stream (Snipetjernsbekken) that ends in a lake (Gjersjøen), which is used for drinking water collection by Nordre Follo and the neighboring Ås municipality. The stream accounts for approximately 6% of the water supplied to the lake.[18] The area under the highway represents the highest topographical point in the studied area, whereas the stream is the lowest point (Fig. 1). Action plans for remediation have been formed, but the implementation is still pending.[22] Information about the local biota at Taraldrud is scarce: the remediation plan for the site states that perch and pike live in the lake, while water fleas have been present in the catchment ponds in the area.[22]

2.2. Sampling

Samples were collected from the area surrounding the alum shale deposit on three occasions: in autumn 2020, summer 2021, and summer 2022. Since this study aimed to assess the transfer and accumulation of leachable elements of concern into different environmental compartments, four sampling points were selected based on the groundwater flow in the area (Fig. 1): reference site (R), precipitation pond (P), mixing zone (MZ), and downstream (DS). Site R was selected upstream from the waste rock to represent the local background of the area. Site P consists of the manmade precipitation pond and the soil in the near vicinity. Site MZ represents an area where the precipitation pond is connected to the stream through a manmade canal. During our sampling campaigns, levels of precipitation were low, and no visible surface water overflow was observed between the pond and stream. Sampling point DS was selected downstream from the deposit to investigate the impact of dilution. An overview of the collected samples at different locations can be found in Table S1.†

Stream water was sampled at 3 of the sampling locations to establish the local background and evaluate the effects of ARD on water quality. Temperature, oxygen concentrations (FDO® 925 Optical Dissolved Oxygen Sensor), pH, conductivity, and oxidation–reduction potential (ORP) of surface waters were measured *in situ* using a portable multi-meter (WTW multi-3420) with appropriate probes. The field ORP measurement was converted to redox potential (E_h) according to instructions from the manufacturer. Additionally, the pH of the precipitation pond water was monitored yearly between 2020 and 2023.

Water samples (unfiltered) for elemental analysis by inductively coupled mass spectrometry (ICP-MS/MS) were collected, transferred to the laboratory, and preserved by acidification to

5% (V/V) with ultrapure concentrated nitric acid (HNO_3) on the same day. Another set of unfiltered water samples were collected but not acidified for total organic carbon (TOC) and anion analyses. To study the mobility and bioavailability of trace elements and radionuclides, on-site water fractioning was performed to distinguish the elemental distribution with particle size. The size fractionation was performed according to Salbu[23] by using an $a < 0.45$ μm membrane filter (polypropylene membrane) and a hollow fiber with a membrane cut-off of 10 kDa (polysulfone membrane). This allows the separation of high molecular mass (HMM), *i.e.*, particulates and colloids, and low molecular mass (LMM) species. Five subsamples were collected from each size fraction and prepared for elemental analysis in the same manner as the unfiltered water samples. All water samples were stored at 4 °C prior to further analysis.

Soil (SO) and sediment (SE) samples were collected using plastic corer tubes, and those from contaminated areas (MZ and P) were collected in duplicate (A and B). No reference sediment sample could be collected from site R. Soil cores were collected by inserting a 30 cm plastic corer tube (ID 11.5 cm) into the soil. Sediment cores were collected from the bottom of the pond by inserting 40 cm plastic tubes (ID 5 cm) into the sediment, which were then capped from the top to form a vacuum, lifted off the ground, and closed from the bottom. The collected soil cores varied in depth between 14 and 20 cm, whereas the sediment cores ranged from 12 to 22 cm. Both soil and sediment cores were sectioned into 2–4 cm resolution before further processing and analysis. Samples were immediately frozen at – 20 °C on return to the laboratory.

Soil porewater (PW) samples from 5 cm depth were collected from the soil cores at sampling site P using Rhizon CSS 5 cm porewater samplers with a membrane (0.15 μm pore size, 5 cm length) connected to a syringe filter to create a vacuum. Samples were acidified to 5% (V/V) using ultrapure concentrated HNO_3 for elemental analysis by ICP-MS/MS. The soil at MZ was dry at the time of sampling and no porewater could be extracted using this method.

Plant samples were collected adjacent to soil and sediment sampling sites in order to permit calculation of elemental transfer factors from soils and sediments to plants. The selection of species was based on the abundance at the sampling locations and the number of plants collected varied depending on type and size in order to have sufficient biomass for analysis (*i.e.*, plants of the same species and location were collected into the same bag and are considered as single representative samples). Samples included European alder and birch leaves, spruce needles, and above-ground biomass and root systems of grass, fern, and aquatic wood club-rush (Table S1†). Samples were transferred to the laboratory on the sampling day and stored at 4 °C until further processing.

Additionally, alum shale (AS) material from 5 locations (Fig. 1 and Table S2†) and of variable particle size (*ca.* 1–30 cm, Fig. S5†) were provided by the Norwegian Geotechnical Institute (NGI) and studied here as the source of contamination at the Taraldrud site. The rock samples had been collected during a drilling and excavation campaign in 2021 (full description and pictures of the conglomerates can be found in a published NGI report[22]). Reported elemental concentrations in waste rock and leachate from location 27 (*i.e.*, closest to samples from site P; Fig. 1) were used to estimate element leachability, whereas the 5 alum shale samples were characterized here for activity concentration of natural radionuclides and mineral phases.

2.3. Solid phase characterization

Dry weight and organic matter content were determined by loss of ignition by using 3 g of field-moist soil and sediment that was first heated to 105 °C and then to 550 °C overnight. After each step, the samples were left to cool down in a desiccator and weighed until stable weight was achieved. Organic carbon content was calculated from organic matter following Krogstad *et al.*[24] The remaining field-moist soil and sediment materials were freeze-dried (epsilon 2–4 LSC) and homogenized. The grain size was determined in the 10–12 cm layers using a wet sieving method as in Reinoso-Maset *et al.*[25] and then categorized using the USDA triangle.[26] Subsamples of the freeze-dried materials were further sieved to <2 mm for pH and cation exchange capacity measurements and ground in an agate ball mill (Restch RM 2000) for total digestion. Soil and sediment pH was measured after allowing the solid material to suspend in ultrapure water for 24 h using a ratio of 1 : 5 (w : V) based on Kalra.[27] Cation exchange capacity (CEC) was measured by using the ammonium acetate (NH_4OAc) method developed by van Reeuwijk.[28]

A subsample (0.2 g) of homogenized solid materials was digested for elemental analysis in a Milestone UltraWAVE using a mixture of ultrapure concentrated HNO_3, phosphoric acid (H_3PO_4, BioUltra ≥85%, Sigma-Aldrich), and fluoroboric acid (HBF_4, 48 wt% in H_2O, Sigma-Aldrich) with a 1 : 2 : 1 ratio at 260 °C for 40 min. This digestion method achieves the full recovery of radionuclides (U and Th by HNO_3, Ra and Ba by H_3PO_4) and targets the silica matrix and refractory oxides with an *in situ* generation of HF by HBF_4. This permitted an easier handling of the solution due to lower toxicity as well as allowing a direct measurement due to the *in situ* generation of H_3BO_3.[29,30] After digestion, the samples were diluted to 50 mL with Milli-Q water, followed by a further 1 : 10 dilution to reduce the concentration of total dissolved solids (TDS) prior to ICP-MS/MS analysis.

Gamma measurements were carried on coarse grain alum shale samples to determine the activity concentrations of natural radionuclides, including K-40, Pb-210, Ra-226, Ac-227, Th-232, U-235, and U-238. To check for potential grain size effect on gamma measurements, a set of subsamples were further crushed, oven-dried at 105 °C, and homogenized in the same manner as soils and sediments prior to digestion and analysis for U and Ra-226 by ICP-MS/MS. Another set of subsamples was further ground in an agate mortar and screened to <60 μm grain size as preparation for mineral phase identification and semi-quantification by X-ray powder diffraction (XRD). A full description of gamma spectroscopy and XRD methods and data analysis can be found in the ESI (Section S1).†

Plant samples were first cleaned by removing any visible soil particles by washing with distilled water. The shoots and roots of the vascular plants were processed and analyzed separately,

but samples of the same species were pooled. Subsequently, the plant materials were oven-dried at 105 °C overnight, homogenized, and digested in triplicate with 5 mL of ultrapure concentrated HNO_3 following the same microwave-assisted digestion as for soils and sediments.

2.4. Aqueous phase analyses

Elemental concentrations of Mg, Al, P, S, Ca, V, Cr, Mn, Fe, Co, Ni, Cu, Zn, As, Mo, Cd, Sn, Sb, Cs, Ba, Th, and U in the acidified aqueous samples were determined in an Agilent 8900 triple quadrupole ICP mass spectrometer using He and O_2 reaction modes. Calibration standard solutions were freshly prepared from single-element ICP standards (Inorganic Ventures®) and Bi, In, and Rh were used as online internal standards during the analysis. To match the matrix of the samples, the calibration standard solutions were prepared in the acid mixture used in the digestions. Radium-226 concentrations were measured in a PerkinElmer NexION 5000 multi-quadrupole ICP mass spectrometer using N_2O reaction mode and Rh-103 as online internal standard (method according to Wærsted *et al.*[30]). The accuracy of the measurements was assessed by measuring a multielement in-house standard solution that was prepared in the same acid mixture as the samples. Additionally, certified and standard reference materials of a similar matrix to the samples and containing the elements of interest (Table S3†) were prepared and analyzed in parallel to the samples in each analysis batch in order to evaluate the accuracy of the method and correct for possible matrix effects. The accuracy of the overall methods (*i.e.*, from sample preparation to digestion and measurement) was acceptable, with elements within ±20% of the certified value (Table S3†). Anion concentrations (F^-, Cl^-, SO_4^{2-}, NO_3^-) in unacidified water samples were quantified by ion chromatography (Lachat IC5000, Zellweger Analytics) and total organic carbon (TOC) was analyzed by a TOC VCPH/CPN analyzer (Shimadzu). A detailed description of the methods can be found in the ESI (Section S1).†

2.5. Data analysis

2.5.1. Leachability of elements from alum shale. Elemental leachability from alum shale was evaluated using the reported alum shale and leachate concentrations (sample AS 27; Fig. 1)[22] following the approach outlined in Tuovinen *et al.*[31] The concentrations in alum shale were divided by the corresponding concentrations found in leachate. The resulting accumulation values were then normalized to the lowest ratio and organized in increasing order. A lower normalized value indicates higher tendency for the element to leach from the source (alum shale) to the adjacent phase (shale leachate). It is worth noting that using leachability for estimating element mobility (*i.e.*, from source to the receiving environment compartment) may comprise an associated uncertainty due to potential mineral heterogeneities, incongruent mineral dissolution, and subsequent reactions by the leached-out elements (*e.g.*, precipitation or sorption).

2.5.2. Enrichment factors. To distinguish between anthropogenically enriched *vs.* natural abundance, enrichment factors (EF) were calculated for water, soil, and sediment as a ratio of normalized elemental concentrations in the sample with respect to the background following eqn (1).[32]

$$\mathrm{EF} = \frac{\left[\frac{C_x}{C_{ref}}\right]_{\mathrm{Sample}}}{\left[\frac{C_x}{C_{ref}}\right]_{\mathrm{Background}}} \quad (1)$$

where C_x is the concentration of the element of interest in the sample or the background, and C_{ref} is the corresponding concentration of the reference element.

The element chosen for normalization should have stable environmental concentrations and be associated with finer soil and sediment particles.[33] Traditionally, elements such as Al, Fe, and Mn are used as reference elements, however, as recommended by Zahra *et al.*,[32] Cs was used for this study due to the formation of ARD. Concentrations measured in samples from site R were used as the local background. When the background concentrations fell below the detection limit (LOD), the method's LOD value was used for the EF calculation. Due to the absence of reference sediment, the reference soil was used for assessing the contamination status in the precipitation pond sediments. Enrichment factors representing different contamination levels for water, sediments, and soils[32,34,35] can be classified as: no enrichment (<1), minor enrichment (<3), moderate enrichment (3–5), moderately severe enrichment (5–10), severe enrichment (10–25) and extremely severe enrichment (25–50). These measured elemental concentrations were also compared to environmental quality standards (EQS) to further estimate the existing risk to aquatic and terrestrial environments.

2.5.3. Transfer factors. To estimate bioconcentration and bioaccumulation in local biota,[36] transfer factors (TF) of natural radionuclides (U-238 and Th-232) were calculated between soils and plants at the Taraldrud site, *i.e.*, sites R, MZ, and P. Transfer factors were calculated from the soil-to-shoot and, when possible, soil-to-root pathways as a ratio of concentrations using an equilibrium-based model following eqn (2):

$$\mathrm{TF} = \frac{C_{plant}}{C_{soil}} \quad (2)$$

where C_{plant} and C_{soil} are, respectively, the concentration (in mg kg^{-1} d.w.) of the radionuclide of interest in plant tissue and in soil from the same site's sampling location.

2.5.4. Radiological risk by the ERICA tool. The ERICA assessment tool[37] was used to assess the radiological risks and absorbed dose rates for the non-human species from the leachable U-238 and Th-232 in the local ecosystem. The ERICA tool is a computer-based tiered approach that allows the user to calculate the total exposure doses based on radionuclide soil activity concentrations and predefined concentration ratios for organisms of interest (see Brown *et al.*[37] for a detailed description). Radium-226 was left out of the assessment based on the low concentrations measured in the environment surrounding the alum shale deposit (see the Results section). Total exposure doses were calculated using the site-specific activity concentrations in the affected environmental media (soil, sediment, water) together with default concentration ratios for reference

organisms using the Tier 2 assessment, which was carried out separately for the stream (aquatic environment), the precipitation pond (aquatic environment), and the soil (terrestrial environment). The estimated dose rates for aquatic plants in the precipitation pond were also evaluated with respect to the assessment performed with measured concentrations in the vascular plant (wood club-rush) collected in the pond. Selected species of biota included a range of ERICA reference organisms that can be expected to be present in the area. The screening value for risk estimation was set to 10 μGy h^{-1} (default value).

2.5.5. Statistics. Principal component analysis (PCA) was used to study the distribution and variation patterns of soil and sediment variables within the contaminated areas (*i.e.*, sites P and MZ). PCA was carried out using R 4.3.1 for standardized and centered data.[38] The dataset included measurements from different duplicate cores (*i.e.*, P-SO(A)-(B), P-SE(A)-(B), MZ-SO(A)-(B)) and all the collected depths. R-SO was excluded from PCA since it represents the local background. Particle size, CEC, mineralogy, and V concentrations were excluded from PCA since the analysis requires a complete dataset for each included sample, as was pH due to its logarithmic scale. Data were visualized using the R packages factoextra,[39] corrplot,[40] and rgl.[41] One-way ANOVA tests were performed to determine the significantly different concentrations in stream water between sampling sites. The non-parametric Kruskal–Wallis test was used to evaluate significant differences between measured average concentrations in soil and sediments as well as in biota collected at the site R. The chosen level of statistical significance was set to $\alpha = 0.05$ for all the analyses.

2.5.6. Geochemical modeling. The PHREEQC computer program (version 3.7.3) was used to model the equilibrium aqueous speciation and solid phase stability[42] in the

Table 1 Geochemistry of surface waters from the reference site (R), precipitation pond (P), mixing zone (MZ) and downstream (DS) of the Taraldrud site. Water parameters were measured *in situ*, whereas anion and elemental analyses were carried out in the laboratory. Sampling campaign years are given in Table S1. Element concentrations are given as average ±1 standard deviation of replicate samples (*n*)

		Sampling locations[a]			
Parameter	Unit	R	P	MZ	DS
T	°C	12	15	12	12
pH		7	3	7	7
Cond.	μS cm^{-1}	426	3257	536	535
O_2	mg L^{-1}	8	12	9	9
E_h	mV	157	402	157	156
TOC	mg L^{-1}	7.4	2.8	7.2	7.4
Anion		***n* = 1**	***n* = 1**	***n* = 1**	***n* = 1**
F^-	mg L^{-1}	0.2	2.7	0.3	0.3
Cl^-	mg L^{-1}	53.2	120	79.2	78.7
SO_4^{2-}	mg L^{-1}	31.2	2100	44.5	45.4
NO^{3-}	mg L^{-1}	0.3	0.1	0.4	0.4
Element		***n* = 3**	***n* = 3**	***n* = 3**	***n* = 3**
Mg	mg L^{-1}	5.8 ± 0.1	123 ± 6	7.1 ± 0.1	7.1 ± 0.01
Al	mg L^{-1}	0.062 ± 0.01	39.7 ± 3.1	0.16 ± 0.06	0.12 ± 0.01
P	μg L^{-1}	<LOD	<LOD	<LOD	<LOD
S	mg L^{-1}	10.1 ± 0.1	697 ± 12	14.9 ± 0.2	14.3 ± 0.6
Ca	mg L^{-1}	43 ± 1	490 ± 10	51 ± 1	50 ± 1
V	μg L^{-1}	0.33 ± 0.03	0.34 ± 0.03	0.33 ± 0.11	0.25 ± 0.01
Cr	μg L^{-1}	<LOD	23 ± 2	<LOD	<LOD
Mn	mg L^{-1}	0.1 ± 0.04	5.3 ± 0.3	0.15 ± 0.07	0.12 ± 0.01
Fe	mg L^{-1}	0.19 ± 0.03	27.3 ± 1.5	0.29 ± 0.15	0.19 ± 0.01
Co	μg L^{-1}	0.13 ± 0.04	307 ± 21	1.24 ± 0.51	0.93 ± 0.05
Ni	μg L^{-1}	1.2 ± 0.2	2200 ± 100	10.1 ± 0.8	9.3 ± 0.4
Cu	μg L^{-1}	<LOD	797 ± 55	<LOD	<LOD
Zn	μg L^{-1}	<LOD	1033 ± 58	<LOD	<LOD
As	μg L^{-1}	0.29 ± 0.01	0.43 ± 0.03	0.29 ± 0.02	0.26 ± 0.01
Mo	μg L^{-1}	2.5 ± 0.1	0.19 ± 0.01	2.5 ± 0.1	2.4 ± 0.02
Cd	μg L^{-1}	<LOD	28 ± 1	0.091 ± 0.026	0.086 ± 0.001
Sb	μg L^{-1}	0.17 ± 0.01	<LOD	0.19 ± 0.02	0.17 ± 0.01
Cs	μg L^{-1}	0.036 ± 0.002	0.22 ± 0.02	0.043 ± 0.009	0.036 ± 0.001
Ba	μg L^{-1}	26 ± 1	12 ± 1	28 ± 1	28 ± 1
Pb	μg L^{-1}	<LOD	8.0 ± 0.7	<LOD	<LOD
Th	μg L^{-1}	0.047 ± 0.006	8.17 ± 0.45	0.055 ± 0.016	0.039 ± 0.002
U	μg L^{-1}	3.2 ± 0.1	843.3 ± 30.6	6.2 ± 0.4	5.8 ± 0.1
Ra-226	ng L^{-1}	<LOD	<LOD	<LOD	n.d.

[a] n.d. = No data available; <LOD = measurement below the method's limit of detection (LOD).

precipitation pond water. The minteq.v4.dat thermodynamic database has been previously applied for acidic drainage systems (as, *e.g.*, in Lee *et al.*[43]), but lacks a comprehensive thermodynamic dataset for radionuclides. Therefore, the database was complemented with published thermodynamic chemical equilibria for relevant Th aqueous complexes as well as ternary uranyl carbonate complexes (Table S4†). Elemental concentrations and water parameters measured in the precipitation pond water (Table 1) together with atmospheric conditions (*i.e.*, equilibrium gas phases at $\log P_{CO_2} = -3.40$ and $\log P_{O_2} = -0.68$) were input in the model. The saturation indices (SIs) expressed as $\log Q/K$ assess the degree of oversaturation (SI > 0), equilibrium (SI = 0), and undersaturation (SI < 0) with respect to a given mineral phase in a given solution. Solution speciation diagrams for U and Th as a function of pH provide with the equilibrium distribution of the prevailing species.

3. Results

3.1. Alum shale characterization and leachability

X-ray diffractograms of alum shale from Taraldrud (Fig. S1 and Table S5†) were strongly dominated by quartz (36–56%), with a significant contribution of aluminosilicate phases (9–22% muscovite, 5–11% orthoclase) and iron sulfate phases (5–22% jarosite, 6–14% pyrite). Calcium sulfate was also contributing to diffractograms of samples 31, 28, and 29, while calcium carbonate reflections were identified in samples 31 and 29.

Activity concentrations of natural radionuclides in the alum shale ranged over two orders of magnitude, with U-238 decay series radionuclides being the highest (Fig. 2 and Table S6†). Sample 29 exhibited the highest activity concentration of U-238, U-235, and Th-232 (1860, 88, and 50 Bq kg^{-1}, respectively), whereas sample 33 presented the highest Ra-226 (2060 Bq kg^{-1}) and Pb-210 (2080 Bq kg^{-1}) activity concentrations. Uranium-238 and Ra-226 activity concentrations determined by ICP-MS/MS were comparable to those acquired from gamma spectroscopy and fell within the same order of magnitude (Fig. S2†), which corroborated homogeneous distribution of radionuclides within the grains and confirms no grain size effect on gamma measurements.

Estimation of elemental leachability from sample AS 27 to the shale leachate resulted in normalized accumulation ratios that decreased as follows: Ba > Pb > V > Mo > As ≈ Cr > Th > Al > Cu > Co ≈ Zn ≈ Cd > Ni ≈ U > S > Fe > Mg > Na ≈ Mn > Ca (Table S7†). This pattern gives an indication of the relative resistance to leach from the alum shale, *i.e.*, the major cations (Ca, Na, Mg), S, Fe, Mn, Ni and U exhibited 100 to 1000 times higher leachability than other metals (Ba, Pb, V, Mo) present in the alum shale.

3.2. Surface water quality

Water quality and chemical composition of surface water samples collected from the stream (at sites R, MZ, and DS) and the precipitation pond (at site P) are presented in Table 1. The pH of the stream water remained consistently circumneutral from site R to site DS, the dissolved oxygen and TOC levels were

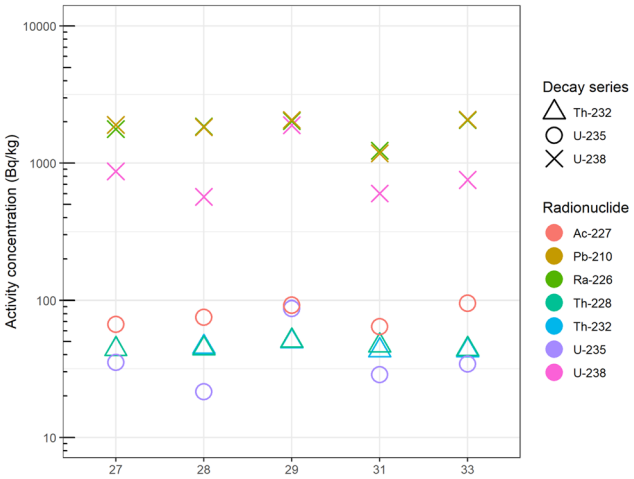

Fig. 2 Radionuclide activity concentrations (Bq kg^{-1} d.w.) in alum shale (AS) from 5 different locations in the Taraldrud site. Numbers on the *x*-axis refer to the AS sample (see Fig. 1 for sampling locations). Radionuclides belonging to different natural decay chains are indicated by different symbols, whereas each radionuclide is marked by different colors. Values and uncertainties can be found in Table S6.†

8–9 and ~7 mg L^{-1}, respectively, and the ORP was 157 mV throughout the sampling points. Only a minor increase in Cl^- and SO_4^{2-}, from 53 to 79 mg L^{-1} and 0.3 to 0.4 mg L^{-1}, respectively, were observed at MZ and DS when compared to site R, whereas the specific conductivity increased about 20% downstream from the mixing zone. Radionuclide concentrations in water samples ranged from 3.2 to 6.2 μg L^{-1} and 0.04 to 0.06 μg L^{-1} for U-238 and Th-232, respectively, whereas Ra-226 was below the limit of detection (*i.e.*, <0.04 ng L^{-1}). The elemental concentrations of Mg, Al, S, Ca, Co, Ni, Cd, Ba, and U were significantly different ($p < 0.05$) at MZ and DS when compared to site R. When the concentrations in sites MZ and DS were compared, only Ca concentrations were significantly different ($p < 0.05$).

The water quality in the precipitation pond was considerably different to that found in the stream (Table 1). The pH in the precipitation pond water has been gradually decreasing over the years 2020, 2021, 2022, and 2023, with measured values being 5.8, 4.4, 3.0, and 2.8, respectively. The specific conductivity and ORP were significantly elevated compared to the stream, exhibiting a 7- and 2.5-fold increase, respectively. Notably, the dissolved oxygen and the levels of anions (Cl^-, SO_4^{2-}, and F^-) were 1.5 to 40 times higher in the pond water compared to the natural background, whereas the TOC and NO_3^- levels were significantly reduced. The elemental concentrations in the precipitation pond water far exceeded those found in the stream at site R, except for Ba and Mo which exhibited lower concentrations. Enrichment factors were calculated for all the elements detected in the pond water (Fig. 3), including for those with concentrations below the limit of detection in the stream water. Calcium, V, As, Mo, and Ba showed no enrichment or minor enrichment, whereas Mg exhibited moderate enrichment and Mn moderately severe enrichment. Sulfur, Cr, and Fe were severely enriched, and Al, Co, Ni, Th, and U as well as those

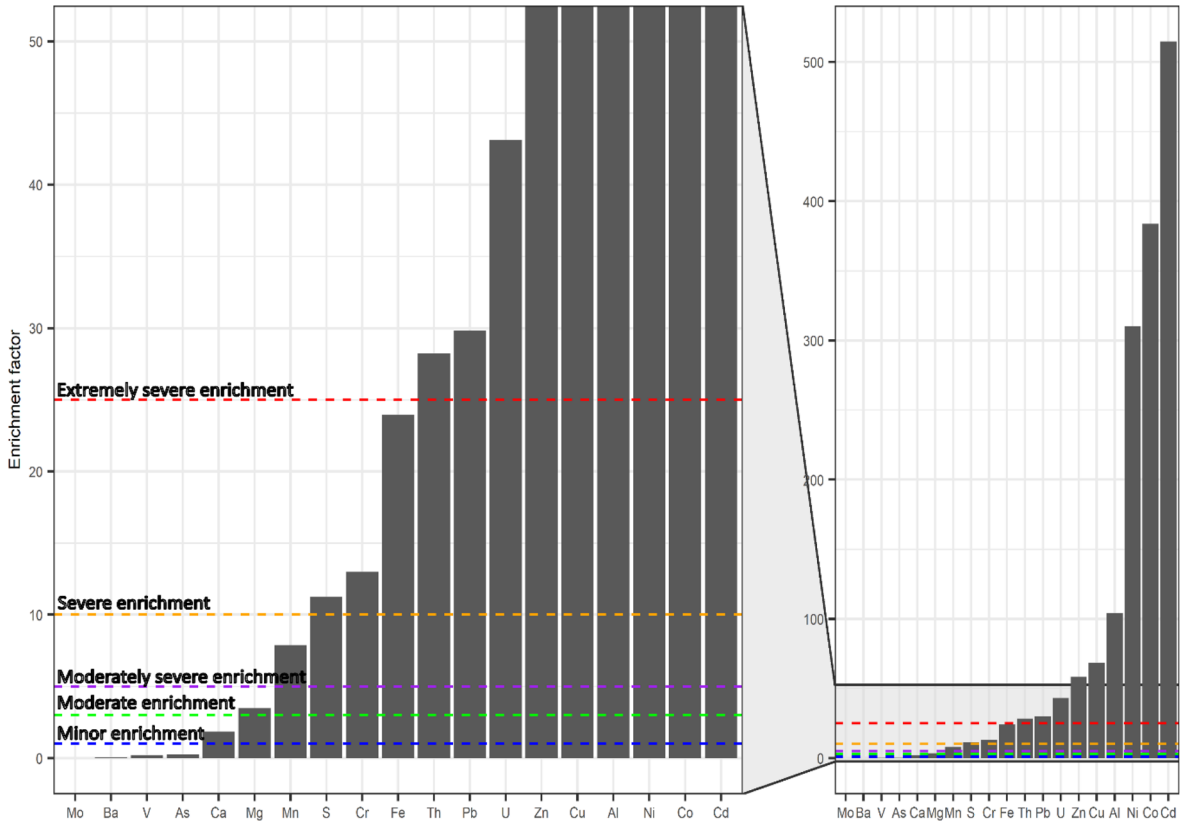

Fig. 3 Enrichment factors (EF) for elements measured in water from the precipitation pond of the Taraldrud site. Colored dashed lines indicate threshold levels for enrichment classification (*i.e.*, minor, moderate, moderately severe, severe, and extremely severe enrichment). EF for Cr, Cu, Zn, Cd, and Pb were calculated using the limit of detection for the method.

undetected in water at site R (*i.e.*, Cu, Zn, Cd, and Pb) were extremely severely enriched. Compared to environmental quality standards (EQS), the concentrations of F, Fe, Cr, Ni, Cu, Zn, Cd, Pb, and U in pond water exceed the allowed concentration limits (Table S8†).

The size distribution in stream water samples from sites R and MZ was somewhat similar (Fig. S3†), with Al, Fe, Th, and V associated with particles and colloids (>10 kDa, HMM), whereas other elements were predominately in the mobile fraction (<10 kDa, LMM). Nevertheless, small differences could be seen between the up- and downstream sites, most significantly the decrease of HMM species in favor of the colloidal fraction. Notably, Al and Ni in stream water at site R were entirely present as particulate and LMM species, respectively, while at site MZ the distribution included 30% colloidal and 20% LMM species for Al and 20% colloidal and 10% particulate for Ni. The size distribution of Fe is also noteworthy as 45–50% was particulate, 35–40% as colloidal, and only 10–15% was present as LMM. The size distribution of elements in the precipitation pond water was different from the stream water, with all measured elements predominantly present as LMM species (except for As and Mo which exhibited a somewhat similar distribution that included 10–15% particulate and 5–10% colloidal fractions, Fig. S3†).

The aqueous speciation of U and Th under the precipitation pond water conditions, *i.e.*, pH 3, was dominated by UO_2SO_4(aq.), UO_2^{2+}, and $UO_2(SO_4)_2^{2-}$ and by $Th(SO_4)_2$(aq.), $Th(SO_4)_3^{2-}$ and $Th(SO_4)^{2+}$ (Fig. S4†). The phase stability assessment showed that the acidic precipitation pond water was oversaturated with respect to several Fe oxy(hydro)oxide phases ($CuFe_2O_4$,

Table 2 Properties of soils (SO) and sediments (SE) from the reference site (R), precipitation pond (P) and mixing zone (MZ) of the Taraldrud site. Results are given as average ±1 standard deviation of replicate samples (*n*). Grain size analysis was carried out on the 10–12 cm depth layer of the soil or sediment

		Soil			Sediment
Parameter[a]	Unit	R-SO	P-SO	MZ-SO	P-SE
		***n* = 7**	***n* = 16**	***n* = 15**	***n* = 16**
pH		4.7 ± 0.4	4.3 ± 1.8	4.7 ± 0.4	3.3 ± 0.5
DW	%	45 ± 9	62 ± 14	45 ± 9	52 ± 21
OM	%	29 ± 5	11 ± 9	30 ± 5	15 ± 11
OrgC	%	17 ± 3	6 ± 5	17 ± 3	9 ± 6
		***n* = 1**	***n* = 1**	***n* = 1**	***n* = 1**
Sand	%	5	7	18	70
Silt	%	46	30	76	28
Clay	%	40	62	6	1
		***n* = 3**	***n* = 7**	***n* = 7**	***n* = 15**
CEC	cmol kg^{-1}	17 ± 3	33 ± 20	51 ± 8	29 ± 17

[a] DW = dry weight, OM = organic matter, OrgC = organic carbon, CEC = cation exchange capacity.

$Fe(OH)_{2.7}Cl_{0.3}$, $Fe(OH)_3$, FeOOH, Fe_2O_3), jarosite ($(H_3O)Fe_3(SO_4)_2(OH)_6$), Mn oxide (MnO_2), anglesite ($PbSO_4$), and barite ($BaSO_4$) (saturation indices can be found in Table S9†).

3.3. Soil and sediment characteristics

The average soil and sediment characteristics of Taraldrud are presented in Table 2. During sampling, yellowish-reddish-brown layers were observed in the MZ and P cores (Fig. S5†). The pH of soils ranged from 4 to 5, while sediments were closer to pH 3 (see also Fig. S6†). The OM content and CEC varied between the sites with MZ-SO soils presenting the highest percentage of organic matter (30%) as well as the highest capacity to retain and exchange positively charged ions (51 cmol kg^{-1}). The soil from site R was classified as loam, the other soils as silty loam, and the sediments as sandy loam.

The average elemental concentrations in soil and sediment cores from sites R, P, and MZ and soil porewater from P-SO core are presented in Table 3. Significant differences in elemental concentrations were observed between the soils from the different sampling locations ($p < 0.05$), while the duplicate cores also showed significant differences ($p < 0.05$) for most elemental concentrations (Table S10†). Generally, the lowest elemental concentrations were found in soils from site R. It is worth noting that the detectable average radionuclide concentrations ranged from 12 to 20 mg kg^{-1} for Th and 3 to 555 mg kg^{-1} for U in soils and sediments and, respectively, 1 and 825 μg L^{-1} in soil porewater, while Ra-226 was below the limit of detection (<7.9–9.6 ng kg^{-1}) in all samples at these sampling sites. The calculated EF showed that U and S are extremely severely enriched in MZ-SO and P-SE samples, and severely enriched in P-SO samples (Fig. 4). Other metals, such as V, Cu, Mo, Cd, Fe, and As, presented severe to moderate enriched concentrations. Compared to quality standards for potentially toxic elements in non-polluted soils and sediments, the measured concentrations of Cu, Cr, Ni, As, Cd, and U in soils and sediments from sites P and MZ exceed the recommended limits (Table S11 and S12†).

The depth profiles for U-238 and Th-232 activity concentration revealed significant variability among the locations (Fig. 5). The Th-232 and U-238 background levels (site R) were 41–71 and 37–60 Bq kg^{-1}, respectively. Compared to these background levels, the Th-232 activity concentration was somewhat higher in soils from the P and MZ sites and sediments from the P site, with similar levels ranging from 45 to 165 Bq kg^{-1}. In contrast,

Table 3 Elemental concentrations in soils (SO), sediments (SE), and porewater (PW) from the reference site (R), precipitation pond (P) and mixing zone (MZ) of the Taraldrud site. Porewater was collected in duplicate from P soil cores at 5 cm depth. Elemental concentrations are given as average ±1 standard deviation of *n* core depths[a]

	Soil			Sediment	Porewater
Element	R-SO (mg kg^{-1})	P-SO (mg kg^{-1})	MZ-SO (mg kg^{-1})	P-SE (mg kg^{-1})	PW (P-SO) (μg L^{-1})
	***n* = 7**	***n* = 16**	***n* = 17**	***n* = 17**	***n* = 2**
Mg	$(9.9 \pm 2.1)\cdot10^3$	$(9.9 \pm 2.9)\cdot10^3$	$(4.7 \pm 2.5)\cdot10^3$	$(7.9 \pm 2.8)\cdot10^3$	n.d.
Al	$(82 \pm 15)\cdot10^3$	$(67 \pm 12)\cdot10^3$	$(61 \pm 19)\cdot10^3$	$(62 \pm 12)\cdot10^3$	$69 \times 10^3 \pm 1.6\%$
S	231 ± 69	$(3.8 \pm 4.7)\cdot10^3$	$(8.3 \pm 9.3)\cdot10^3$	$(10 \pm 8.6)\cdot10^3$	$680 \times 10^3 \pm 1.4\%$
Ca	$(8.2 \pm 1.2)\cdot10^3$	$(9.9 \pm 4.9)\cdot10^3$	$(4.1 \pm 2.5)\cdot10^3$	$(7.5 \pm 2.3)\cdot10^3$	$265 \times 10^3 \pm 1.8\%$
Cr	87 ± 27	77 ± 7	63 ± 19	91 ± 12	$17 \pm 1.3\%$
Mn	892 ± 125	466 ± 191	204 ± 103	316 ± 108	$6100 \pm 1.4\%$
Fe	$(40 \pm 8.7)\cdot10^3$	$(79 \pm 46)\cdot10^3$	$(138 \pm 154)\cdot10^3$	$(132 \pm 58)\cdot10^3$	$150 \times 10^3 \pm 1.0\%$
Co	15 ± 3	15 ± 8	9 ± 2	10 ± 3	$500 \pm 2.5\%$
Ni	41 ± 13	79 ± 50	65 ± 29	75 ± 30	$3650 \pm 2.6\%$
Cu	23 ± 6	105 ± 66	177 ± 147	216 ± 205	$1095 \pm 2.0\%$
Zn	111 ± 23	150 ± 76	104 ± 52	107 ± 38	2400 ± 1.3
As	5 ± 3	9 ± 2	18 ± 19	14 ± 5	$0.1 \pm 3.3\%$
Mo	2 ± 1	10 ± 6	24 ± 31	18 ± 9	$0.01 \pm 34\%$
Cd	0.15 ± 0.04	0.60 ± 0.66	0.89 ± 0.57	0.33 ± 0.39	$49.0 \pm 1.2\%$
Sn	3 ± 1	5 ± 1	2 ± 1	3 ± 1	n.d.
Sb	<LOD	<LOD	<LOD	<LOD	$0.02 \pm 14\%$
Cs	4.4 ± 0.8	4.4 ± 0.6	4.7 ± 2.7	3.7 ± 1.0	$0.1 \pm 6\%$
Ba	733 ± 111	732 ± 82	446 ± 252	744 ± 170	$3 \pm 2\%$
Pb	0.05 ± 0.07	0.04 ± 0.01	0.02 ± 0.01	0.04 ± 0.01	$0.10 \pm 6.3\%$
Th	12 ± 3	16 ± 9	20 ± 5	19 ± 7	$1 \pm 2\%$
U	3 ± 1	48 ± 34	555 ± 641	210 ± 277	$825 \pm 2\%$
	***n* = 4**	***n* = 14**	***n* = 13**	***n* = 16**	***n* = 2**
V	12 ± 2	124 ± 18	114 ± 30	162 ± 22	$6 \pm 2\%$
	***n* = 3**	***n* = 3**	***n* = 3**	***n* = 6**	***n* = 2**
Ra-226	<LOD	<LOD	<LOD	<LOD	<LOD

[a] n.d. = No data available; <LOD = measurement below the method's limit of detection (LOD).

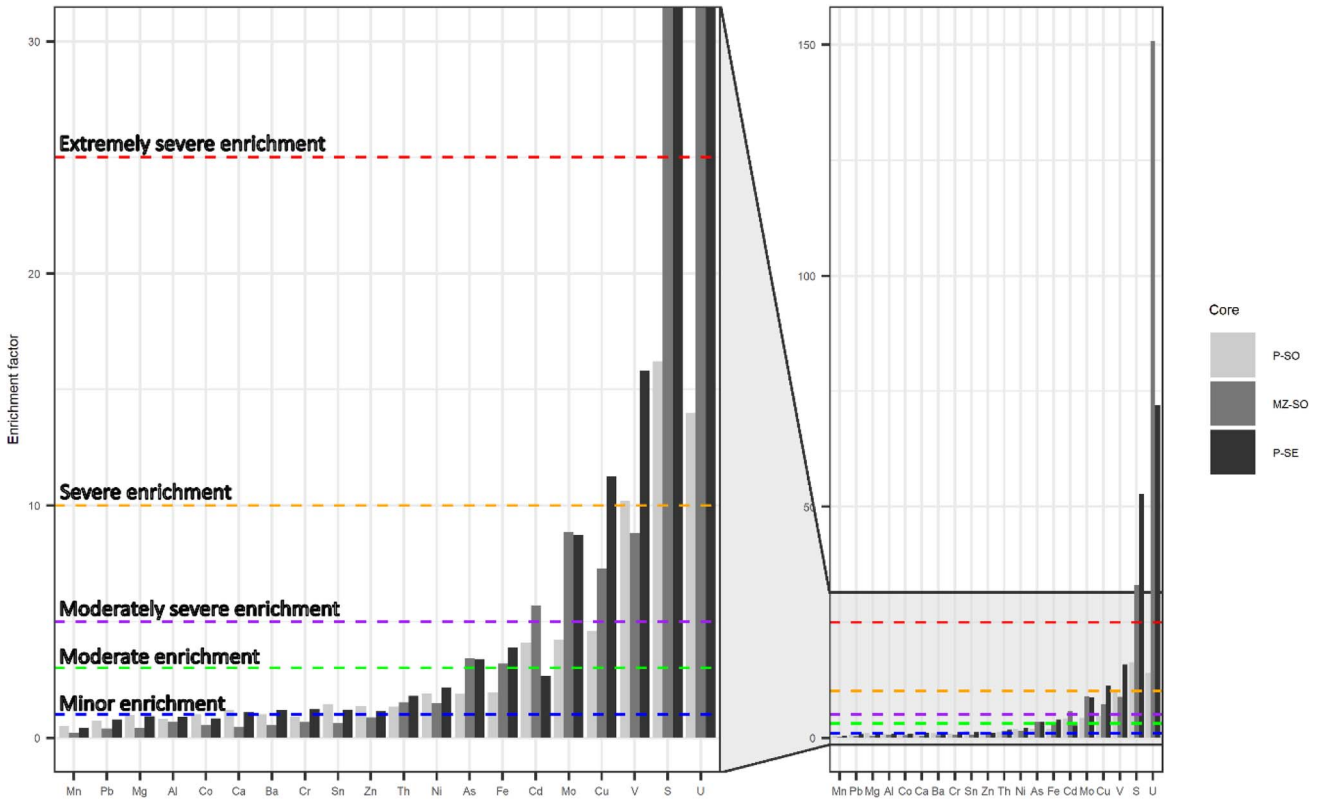

Fig. 4 Enrichment factors for elements measured in soils (SO) and sediments (SE) from the mixing zone (MZ) and precipitation pond (P) of the Taraldrud site. Colored dashed lines indicate threshold levels for enrichment classification (*i.e.*, minor, moderate, moderately severe, severe, and extremely severe enrichment).

U-238 in soils and sediments exhibited an important enrichment above the background levels, with over 2 orders of magnitude higher activity concentrations (~100 to 20 000 Bq kg^{-1}). The highest concentrations were generally in the surface layers, reaching a maximum of *ca.* 25 800 Bq kg^{-1} at 4 cm depth at site MZ. Interestingly, the depth profile of both radionuclides matched in the soil and sediment cores of site P with lower activity concentrations deeper than 10 cm, whereas one of the MZ cores showed a significant increase in Th-232 and U-238 activity concentration at 14 cm or deeper.

Multivariate analysis resulted in the first four principal components (PC1–PC4) with eigenvalues greater than 1 which explained 87% of the total variation within the data set (Fig. 6, S7, S8 and Table S13†). PC1 explained 49% of the variation and had negative loadings with S concentrations. The PCA biplot shows that higher the S concentrations, higher the Fe, Cu, As, Mo, and U concentrations, while lower S concentrations were associated with key lithogenic elements (Mg, Al, Mn, Sn, Cs, Ba) and an increase in soil/sediment dry weight (DW) fraction. PC2 accounted for 21% of the variation and had strong negative loadings with Ca, Mn, Co, Ni, Zn, Cd, and Pb. PC3 and PC4 constituted 10 and 7% of the total variation, respectively. PC3 had strong negative loadings with Cr and Th and a slightly weaker one with organic C, whereas PC4 had strong positive associations with S, Cr, and Fe and strong negative ones with Cs and organic C. The first four PCs were subsequently plotted against their potential explanatory variables (Fig. S9†) and resulted in a linear correlation between PC1 and S concentration, a weaker correlation between PC2 and soil/sediment pH (mainly at pH < 6), and no clear correlation between PC3 and PC4 with soil organic matter. Additionally, the heterogeneity within each soil and sediment core was further investigated by plotting the depth profiles of PC1, PC2, and PC3 scores in a three-dimensional plot (Fig. S10†), which showed differences in loadings and PC correlations between the upper (0–12 cm) and deeper (12–22 cm) layers.

3.4. Transfer factors and radiation doses

For all biota samples, the activity concentrations of U-238 and Th-232 were generally higher in the roots than in the shoots (Table S14†). Wood club-rush from site P had the highest U-238 concentrations in shoots and roots (7.8 and 153 mg kg^{-1} d.w.), among all species, with exception of the roots of grass from site R and MZ that presented 413 and 325 mg kg^{-1} d.w., respectively. The highest Th-232 activity concentrations were found in the shoots of grass and in the roots of wood club-rush both from site P, reaching 0.29 and 3.6 mg kg^{-1} d.w., respectively. Significant differences in the uptake of U-238 and Th-232 ($p < 0.05$) were observed between the sites for grass shoots, grassroots, fern roots, spruce buds, birch leaves, and European alder leaves, whereas fern shoots showed no difference in uptake ($p > 0.05$). Wood club-rush was only found in the precipitation pond and hence no comparison could be made between different

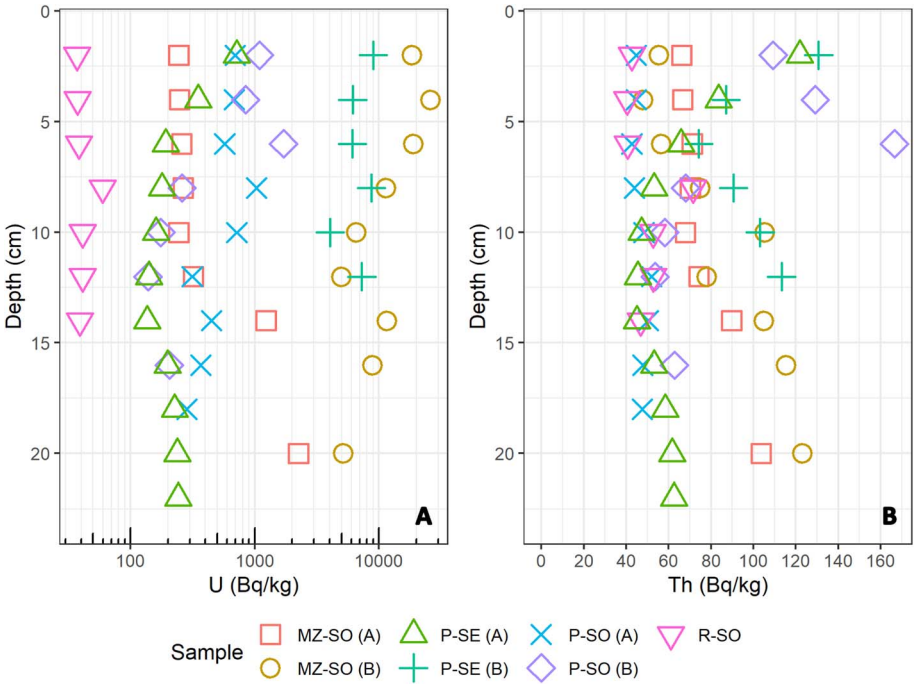

Fig. 5 Activity concentration depth profile in soils (SO) and sediments (SE) of the Taraldrud site. Activity concentrations (in Bq kg^{-1} d.w.) of (A) U-238 and (B) Th-232 are shown for duplicate cores sampled at the precipitation pond (P) and mixing zone (MZ) sites and one core from the reference site (R). Note the logarithmic scale in the *x*-axis in (A).

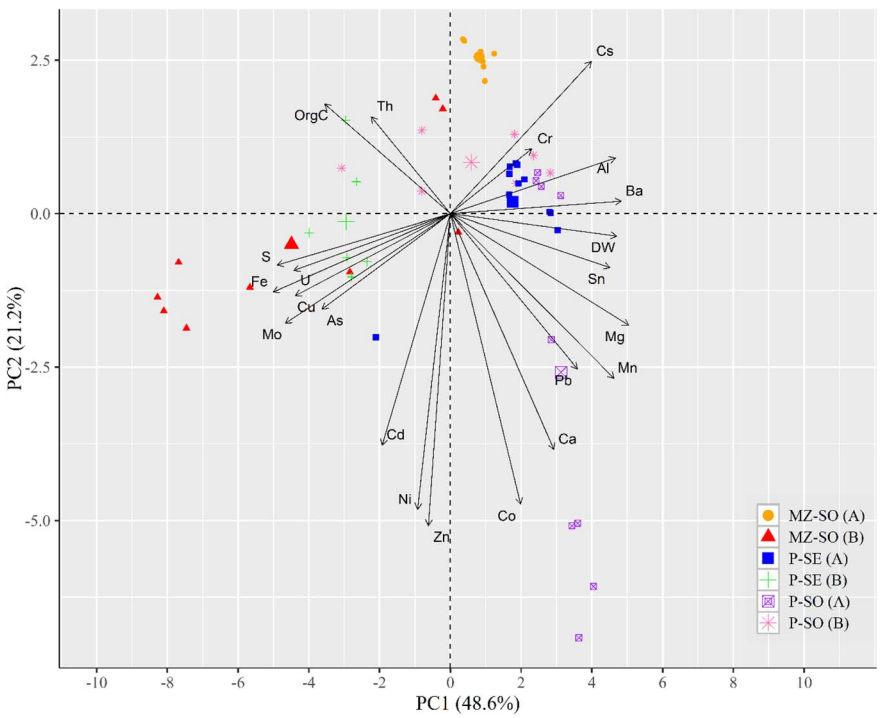

Fig. 6 Principal component (PC) biplot of the characterization results for soils (SO) and sediments (SE) from the precipitation pond (P) and mixing zone (MZ) of the Taraldrud site. The direction of the arrow indicates the negative/positive contribution of the variable to the first two factors (PC1–PC2), while the length of the arrow represents the weight of this contribution. The location of the individual data points indicates how the samples relate to the PC. Each data point corresponds to a different core depth, different symbols represent the different soil and sediment cores. The average score (barycenter) of each core sample group is represented by a larger symbol.

contamination levels. Despite the high activity concentrations in soils, calculated soil-to-shoot TF were generally low, ranging from 4.1×10^{-5} to 5.7×10^{-1} for U-238 and from 9.5×10^{-4} to 2.5×10^{-2} for Th-232 (Table S14†). Soil-to-root transfer was higher than soil-to-shoot for all plant species, with TF values from 3.8×10^{-3} to 1.2×10^{2} for U-238 and from 3.8×10^{-2} to 1.5×10^{-1} for Th-232 (Table S14†). No clear relationship between plant species and soil activity concentrations could be seen.

Estimated total absorbed dose rates for non-human biota from the stream water were all below the set screening dose rate of 10 μGy h^{-1} from U-238 and Th-232 (Fig. 7A). On the other hand, the screening dose rate exceeded for annelids, arthropods (detritivorous), grasses and herbs, lichen and bryophytes, mollusk (gastropods), and shrubs in terrestrial environments at sites P and MZ (Fig. 7B). The aquatic environment of the precipitation pond presented the highest total dose rates of all the studied compartments, with values exceeding the screening dose rate for all the organisms, except for amphibians (Fig. 7C). However, when the total dose rates were estimated using the measured site-specific activity concentrations of U-238 and Th-232 in aquatic plants (wood club-rush), instead of the available CR values within the tool, the total dose rate for vascular plants fell from 184 μGy h^{-1} to 3 μGy h^{-1} (*i.e.*, below the screening level). Overall, the internal dose rates dominated over the external ones and the highest contributor to the estimated total dose rate was U-238.

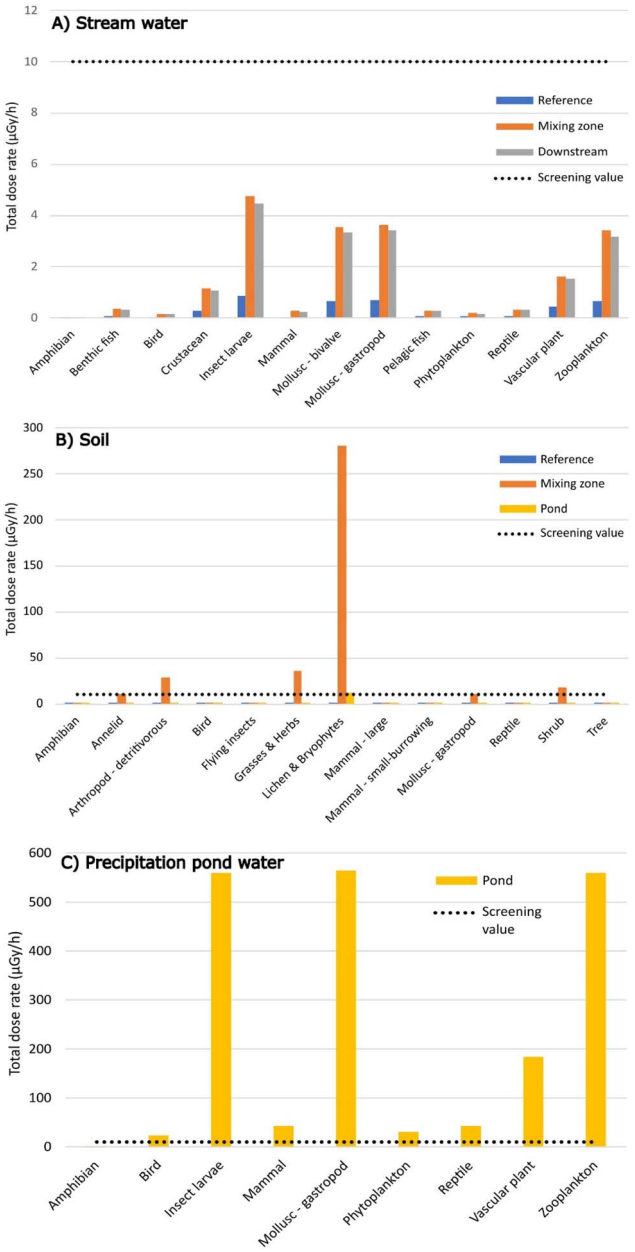

Fig. 7 Total dose rates from U-238 and Th-232 per reference organism in stream water (A), soil (B), and precipitation pond water (C) estimated by the ERICA tool. Total dose rates for each organism are given in μGy h^{-1}. The dotted lines indicate the screening level.

4. Discussion

4.1. Environmental processes due to ARD

4.1.1. On-going alum shale weathering. The elevated environmental concentrations of leachable elements together with the observed increase of electrical conductivity and oxidation–reduction potential, and the decrease of environmental pH suggest on-going formation of ARD at Taraldrud. Parts of the waste rock have been previously classified as non-acid producing,[22] however, the observed disequilibrium within the natural U decay chains (Table S6,† see Section 4.1.3) indicates that the alum shale waste rock is weathering. Therefore, there may also be formation of neutral rock drainage (NRD), generated from neutralization by acid-consuming minerals,[9,14] such as the Ca carbonate identified in the alum shale (Table S5†). The environmental contamination derived from alum shale is influenced by mineral composition,[11] thus the elements forming the main minerals in alum shale waste rock from Taraldrud (*i.e.*, Si, Ca, Al, K, Fe, Ba; Table S5†) can provide insights on the weathering processes.

The observed high degree of S and Fe leachability (Table S7†) and high concentrations measured throughout the site (Tables 1, 3 and S5†) indicate the weathering of alum shale by oxidation and dissolution of pyrite (FeS_2) (Table S5†). This process is supported by the presence of secondary sulfate phases as jarosite in the alum shale (Table S5†) and the decrease of nitrate concentrations in the precipitation pond water (Table 1), as nitrate can be utilized as an electron acceptor during pyrite oxidation. The notably high enrichment of S and Fe found in the pond sediments and mixing zone soils suggests the formation of secondary sulfate phases, such as gypsum (calcium sulfate dihydrate) observed in mine sites affected by acidic leachates from pyrite oxidation,[44] and/or Fe rich phases, such as secondary Fe minerals formed from sulfide oxidation.[45] The precipitation of Fe oxides (hematite, maghemite), hydroxides (ferrihydrite), oxyhydroxides (lepidocrocite, goethite), and oxyhydroxysulfates (jarosite) was thermodynamically favorable under the pond water conditions (Table S9†), which is further supported by the differences in size distribution (Fig. S3†). In the stream water, Fe was mainly in the form of colloids and particulates, whereas low molecular mass Fe species dominated in the precipitation pond water. This indicates that Fe has been

precipitating and accumulating in the pond sediments and mixing zone soils before reaching the stream. These newly formed secondary phases might act as a sink for metals and radionuclides leached during ARD.

4.1.2. Release and retention of potentially toxic elements. Taraldrud is a complex multi-stressor site, where multiple potentially toxic elements are leachable from the alum shale waste rock. Considering that the ARD runoffs follow the groundwater flow driven by the local topography (Fig. 1), the measured soil porewater concentrations (Table 3) were in good agreement with the estimated leachability of the elements (Table S7†). Once released, these elements exhibited different environmental behaviors that strongly depended on the prevailing environmental pH conditions. Soils surrounding the precipitation pond had on average higher pH (circumneutral) than sediments in the pond (acidic), likely explained by ARD input. Yet, multivariate trends were seen by PCA, which led to different explanatory variables driving the release and retention of leachable elements.

The strong negative association of PC1 with S concentration suggests the precipitation of sulfate phases, which dominated the retention processes in the mixing zone soils and the pond sediments. Based on the measured sulfate concentrations, the leached elements could be grouped into those possibly associated with sulfate phases (Cu, As, Mo) and those possibly associated with the soil inorganic fraction (Al, Mn, Ba, Cr). Copper presented high leachability (with slightly higher porewater concentrations compared to precipitation pond water) but also moderate to severe enrichment in pond sediments and mixing zone soils (Fig. 4). Similarly, the low levels of leached out As, Mo and V (Table S7†) were strongly retained in soils and sediments throughout the site (Fig. 4), but the enrichment in the pond water was minor compared to Cu levels. Indeed, the pond water contained Cu mainly as LMM while As, Mo and V had a significant fraction of colloids and particulates. Yet, the levels in the stream water remained below the detection limit (Cu) or were similar to those found in the pond (As, Mo, V). Overall, there was an effective immobilization of these elements in the ARD impacted soils and sediments. Although seasonal dry periods could enhance leachability[14] and formation of colloids could aid with the mobility of these elements,[23] the high retention is likely occurring due to co-precipitation with newly formed secondary Fe oxyhydroxides or hydroxy sulfate phases during the on-going ARD, as reported for an alum shale deposit in Sweden,[46] or through pH-dependent adsorption.[47] The secondary Fe mineral phases commonly formed from sulfide oxidation have a small particle size combined with a large surface area, providing excellent sorption sites for leachable elements such as V and As.[45] Copper also presents a moderate sorption affinity for secondary Fe oxides.[48] Therefore, despite the different leachabilities of these elements, the formation of secondary iron and sulfate phases is driving their retention within the soils and sediments at the Taraldrud site.

Aluminum is a significant component in alum shale, typically occurring within aluminosilicate minerals[45] such as the muscovite and orthoclase identified in Taraldrud's waste rock (Table S5†). Despite the partial mobilization of Al from the alum shale and very low enrichment in soils and sediments, it leads to high concentrations in porewater and extremely severely enriched pond water. Interestingly, ~97% of the Al was present as mobile LMM species, whereas in the stream water Al was mainly associated with the HMM fraction. This can be explained by the pH-dependent chemistry of Al, with precipitation occurring under neutral conditions, while readily soluble Al sulfate species are formed under acidic conditions (*e.g.*, $AlSO_4^+$, $AlSO_4^{2-}$).[45] The mobility of Cr is also pH dependent; positively charged species dominate under acidic conditions,[49] in agreement with the high fraction of LMM species measured in the precipitation pond water (Fig. S3†), while oxyanion species (CrO_4^{2-}) can form in circumneutral oxidizing environments,[50] such as those on site MZ. Similarly, the readily leached Mn from the alum shale was not retained in the soils or sediments but remained dissolved in the pond water. This moderately severe enrichment is likely due to the inhibited formation of Mn-oxides and stabilization of Mn^{2+} in solution under the acidic conditions of the pond.[51] Barium exhibited the lowest leachability of all the investigated elements (Table S7†), in agreement with the low concentrations in soil porewater and low enrichment factors throughout the site. High sulfate concentrations can limit the mobility of alkaline earth elements; once the saturation point is reached, $BaSO_4$(s) starts to precipitate (Table S9†), which in turn can act as a scavenger of Ra (see Section 4.1.3).

Elements that had strong negative associations with PC2 (Ca, Co, Ni, Zn, Cd) were seen as most dominant in precipitation pond soils, which had circumneutral pH within the top 10 cm. These top layers formed their own cluster in the 3D PCA plot (Fig. S10†) away from the other points, which suggest a pH-dependent retention; these elements were generally highly enriched in the pond water (as LMM species) rather than in the soils and sediments. For example, Ca showed minor or moderate enrichment within the studied environmental compartments despite the high leachability from the alum shale. This could mean that the saturation of $CaSO_4$ in the surface waters did not exceed the solubility limit as no precipitation was observed under the circumneutral or acidic conditions.[45] Cobalt, Ni, and Zn exhibited similar environmental behavior, with an estimated leaching ability comparable to that observed during bioheapleaching of black shale (Ni > Zn ≈ Co)[31] and extremely high levels in the pond water, even 1.5–2 times higher in soil porewater but lower in the soils and sediments (Fig. 4). This low retention may be explained by the positive net charge of the Fe-rich minerals under acidic conditions that favor the adsorption of negatively charged species rather than cationic species. Contrastingly, Cd concentration was twice as high in the pond water than in the soil porewater and some enrichment in the soils was observed compared to the minor enrichment in sediments. This difference in retention could be explained by the weak binding ability of Cd^{2+} with OM, clay, or oxide minerals in well-drained acidic soils.[52]

4.1.3. Radionuclide remobilization. During the weathering of the waste rock and formation of ARD, the U present in the alum shale is being greatly mobilized, as indicated by the Ra-226/U-238 and Ac-227/U-235 disequilibrium in most of the samples (Table S6†). The only exception is in location 29, where

secular equilibrium was observed, which is in agreement with the previously reported classification of unweathered alum shale without acid-forming potential.[22] Waste rock from location 28 has also been categorized as non-acid-forming alum shale.[22] However, our results show that there is a U-238/Ra-226 disequilibrium, thus the release of radionuclides could also be attributed to the formation of NRD.[53]

Uranium presented relatively high leachability from the alum shale, and it was seen in extremely severely enriched concentrations in most environmental compartments at Taraldrud. In the precipitation pond water, the high dissolved oxygen levels together with high total Fe and low TOC concentrations (Table 1) indicate prevailing oxic conditions since reducing natural waters in high Fe are uncommon unless organic matter decomposition occurs.[54] These oxic, acidic conditions of the pond water likely result in the formation of uranyl species (oxidized U) encompassing UO_2^{2+} and sulfate complexes ($UO_2SO_4^0$, $UO_2(SO_4)_2^{2-}$) (Fig. S4†). These readily mobile uranyl sulfate complexes are often seen under acid-mine conditions.[55,56] In the soils and sediments from the pond and mixing zone, the high U concentrations can be explained by its adsorption affinity onto mineral phases, such as Fe and Mn oxy(hydr)oxides, sulfides, and phyllosilicates.[57] If anoxic conditions have developed in the deeper soil and sediments, U could have also undergone incorporation into ferric oxy(hydr)oxide mineral phases through the Fe-cycling (*i.e.*, reductive dissolution of Fe(III) to more soluble Fe(II) followed by reoxidation to Fe(III) and co-precipitation with U).[58] Another explanation could be adsorption to soil organic matter, which is rather high in soils and sediments at Taraldrud. Fuller *et al.*[59] showed that the U–organic interactions resulted in the formation of strong and reasonably stable complexes with reduced mobility.

The secular equilibrium observed between Pb-210 and Ra-226 and no detectable (Ra) or generally low (Pb) concentrations found throughout the site suggests very low leachability of these U-238 progeny nuclides from the alum shale waste rock. Any release of these radionuclides could have been readily immobilized by the formation of secondary sulfate phases (Table S9†). The precipitation pond water was slightly oversaturated with respect to barite ($BaSO_4$), which can act as a Ra scavenger, and with respect to anglesite ($PbSO_4$), which readily precipitates due to excess SO_4^{2-} in ARD leachates.[60]

Based on the observed isotopic ratios (Table S6†) and calculated enrichment factors (Fig. 4), Th presented higher leachability than Ra and Pb. When compared to background levels, the highest Th concentrations were found in the precipitation pond water (classified as extremely severely enriched), whereas no enrichment was seen in the soils and sediments or in the stream water. The acidic (pH ~3), oxidizing conditions and high excess of dissolved sulfate of the pond water favors the formation of aqueous hydroxides and sulfate complexes,[61] *i.e.*, $Th(SO_4)_2$, $Th(SO_4)^{2+}$, and $ThOH^{3+}$ species (Fig. S4†), which is in a good agreement with the observed size fractionation dominated by LMM species (Fig. S3†). The low clay content in the sediments of site P and soils of site MZ (Table 2) may have diminished the retention of these Th species from the water flow towards the stream, and under circumneutral conditions they are less prone to strongly adsorb onto organic matter and mineral particles (*e.g.*, schwertmannite, an Fe-oxyhydroxysulfate) than anionic sulfate species, such as $Th(SO_4)_3^{2-}$.[54,61]

4.2. Environmental implications

4.2.1. Radiological risk. Overall, elevated concentrations of U and Th were measured in the different environmental compartments at the Taraldrud site, the majority of which surpassed legislated guideline values. Although the activity levels in the waste rock fall within reported values for alum shale in Scandinavia (U-238, Th-232) and Norway (Ra-226, Pb-210),[14,62] measured activity concentrations were above the 1000 Bq kg^{-1} limit for Ra-226 and Pb-210 (all locations) and for U-238 (unweathered alum shale, location 29) to be considered low-level radioactive waste,[63] in contrast to previously reported values setting the waste rock below regulatory limits.[22] Soil from the reference site closely resembled the world average values for U-238 (33 Bq kg^{-1}) and Th-232 (45 Bq kg^{-1}),[64] while soils and sediments from the ARD-impacted areas significantly surpassed these levels (Fig. 5). As well as the mixing zone soils, certain soil and sediment depth layers in the precipitation pond exceeded the recommended limit for U in soils (Table S11†) and the 1000 $Bq_{U\text{-}238}$ kg^{-1} limit for low-level radioactive waste.[63] Moreover, the pond water levels were >50 times higher than the current environmental quality standards for U (Table S8†), and it could be assumed to be critical also for Th with 160 times higher concentrations than in the stream water (no available published quality standard for Th). Uranium and Th concentrations in the stream water were above the world average (0.083 and 0.012 μg L^{-1}, respectively),[64] but fall within the range for European freshwater streams (<10 and 0.1 μg L^{-1}, respectively)[54] and are below the safe drinking water guideline values set by the World Health Organization.[65] Nevertheless, this enrichment of U throughout the site, enhanced Th levels in the precipitation pond water, and the high percentage of potentially bioavailable species in the pond water for both radionuclides (>95% as LMM, Fig. S3†) may cause health and environmental concern since U is both a radiologically and chemically toxic substance for biota and humans[66] and Th may undergo bioconcentration in lower trophic aquatic organisms (*e.g.*, algae).[61]

The radiological risk assessment resulted in no radiological risk for organisms living in the stream but those in the precipitation pond received the highest estimated risk (Fig. 7), as expected from the measured U-238 and Th-232 activity concentrations in these aquatic environmental compartments. In the terrestrial environments, only lichen and bryophytes in the pond soil were estimated to reach the screening value, while annelids, arthropods (detritivorous), grasses, herbs, lichen, bryophytes, mollusk (gastropods), and shrubs in the mixing zone were estimated to be under risk. This radiological exposure agrees with all the U-238 and Th-232 concentrations in the biota (Table S14†) falling above UNSCEAR reference values for leafy plants (0.004 and 0.005 mg kg^{-1}, respectively).[64] Notably, U concentration in the wood club-rush of the precipitation pond was 1 order of magnitude higher than values previously reported in abandoned uranium mining and milling sites in Germany.[67] In agreement with previous studies,[68,69] the

accumulation in the shoots was lower than in the roots; yet, the calculated transfer factors for U-238 and Th-232 were generally low. The lowest accumulation of U in plant shoots was observed at the site MZ, where the soil had the highest fraction of sand but also the highest CEC, OM, and Fe content among the sampling sites (Table 2). Thus, the MZ soils exhibited an enhanced retention capacity due to the presence of organic and mineral phases with high reactive surfaces. In contrast, soils from site P were predominated by the clay fraction (*i.e.*, high sorption capacity for metals and radionuclides[70]) that seemed to control the uptake of Th into plants (lowest TF for most plants). Moreover, the presence of complexing agents, such as sulfate (in excess in the contaminated surface waters), may have enhanced the sorption of U and Th neutral/positively charged complexes (Fig. S4†) onto negatively charged surface sites of the sandy soils,[71,72] clays, organic matter and/or Fe phases. The prevailing aqueous speciation can also reduce the plant's affinity for these radionuclides,[73] resulting in a hindered bioaccumulation. Overall, the bioaccumulation of U was slightly higher than the uptake of Th, likely due to the higher solubility and mobility of U and its ability to mimic essential elements.[74]

Utilizing site-specific concentration ratios instead of the default gives more accurate estimates of the prevailing risks by naturally occurring radionuclides at contaminated sites. Oughton *et al.*[75] reported two orders of magnitude lower dose rates from U concentrations measured in aquatic plants, a similar decrease to that observed in our risk assessment when considering the site-specific concentrations for aquatic wood club-rush. In our study, the limited number of measured concentrations in biota and the lack of natural progeny radionuclide activity concentrations may have incurred higher uncertainty. Therefore, further radiological risk assessments should include all the radiologically important naturally occurring radionuclides. It is also worth noting that the ERICA tool only considers the radiological effects, thus the risk may be underestimated if the element is also chemically toxic, such as U.[76]

4.2.2. Environmental impact. On-going ARD without effective mitigation measures can cause complex environmental impacts, affecting water quality, soil health, and ecosystem functioning. The complexity can derive from a wide range of processes mobilizing and accumulating the potentially toxic elements of concern differently under the prevailing conditions at the environmental compartments.

The water quality of stream at the Taraldrud site currently complies with environmental quality standards (Table S8†). The slightly higher Cl^- and SO_4^{2-} concentrations and conductivity measured in the downstream area may be associated with a slow infiltration of precipitation pond water. Nevertheless, the concentration of anions and TOC were fairly similar to those previously measured in a nearby stream.[34] Other measured elements were at comparable levels to those previously reported in Norwegian streams and rivers (*i.e.*, Mg, Ca, Cr, Mn, Co, Ni, Cu, Zn, As, Mo, Cd, Sn, Ba, Pb) or even lower than previously reported for freshwater in the area (*i.e.*, Al, Fe, V).[34,77] The only element exceeding both the natural background and the environmental quality standard was Ni (Table S8†), which may pose a risk to the aquatic organisms living within the stream. Nickel levels were also over the regulatory limits in the impacted soils (Table S11†) and sediments (Table S12†). Moreover, the Cr, Cu, and As concentrations in all impacted soils were over the standards for non-polluted soils, with Cr and Cu exceeding the levels even at the reference site (natural high background). In impacted sediments, Cr, Cu, Zn, and Cd exceeded the concentration threshold for ecological risk. Since the environmental pH at Taraldrud ranged from slightly acidic (pH 5) to acidic (pH 3), it can be assumed that most of the minerals present in the impacted soils and sediments have a net positive charge, favoring the adsorption of negatively charged species (*e.g.*, oxyanions of As and Mo). For example, the newly formed secondary Fe oxyhydroxide minerals due to ARD would have a positively charged surface with decreasing pH[53] and thus enhance the retention of potentially toxic elements in soils and sediments. Nevertheless, under the acidic environmental conditions at the Taraldrud site, sulfate is most likely the dominant ligand affecting retention, either through complexation, precipitation, or competitive adsorption.[44,45]

The pond water may present the highest ecological risk among the environmental compartments of the Taraldrud site. Many of the leachable elements of concern (*e.g.*, Cr, Fe, Ni, Cu, Zn, Cd, Pb, Mo, As) were present in high concentrations, exceeding both the natural background and environmental limits (Table S8†). The Fe, As, and Mo levels were in line with those measured in a pit lake in a legacy alum shale mine at Kvartorp, Sweden, while the levels of Ni, Zn, Cd, Pb, and U closely resembled those found in contaminated groundwater in the same area.[5] Water conductivity at Taraldrud's precipitation pond was *ca.* 3 times higher than that reported for disposal water in another Norwegian alum shale disposal site,[14] likely due to a significant Cl^- input from the use of salt as a de-icing measure on the adjacent road. Interestingly, the elements enriched in the pond water were present mainly as LMM species, which may lead to the accumulation in local biota. The size distribution of the elements is key for understanding and predicting short- and long-term consequences[78] since LMM species represent the mobile and potentially bioavailable fraction (*i.e.*, available for uptake by organisms). The high percentage of LMM in the pond water is consistent with the on-going ARD formation because most elements within ARD would be present as metal ions or complexed by sulfates.[45] Although colloids are not considered as mobile as LMM. the increase of the colloidal fraction in stream water by the mixing zone area may indicate an enhanced remobilization of contaminants downstream likely due to complexation by refractory humic substances.[79] Overall, the water quality was significantly different between the stream and pond, which was expected since the precipitation pond was constructed to mitigate contamination.

As a mitigation strategy, liming materials (*i.e.*, most common being calcium carbonate ($CaCO_3$), calcium/magnesium carbonate ($CaMg(CO_3)_2$), calcium oxide (CaO_2) and calcium hydroxide ($Ca(OH)_2$)) have allegedly been periodically used at Taraldrud to control the pH in the precipitation pond water.[18] An increase of pH can remove soluble Al, Zn, Ni, and Cd species from solution[45,79] and contribute to the precipitation of Mn oxides, which are known to retain Ba, Pb, and Zn.[59,80] However, a change from acidic to circumneutral pH pivots the net surface

charge of minerals from positive to negative. This in turn can increase the mobility of negatively charged elements, such as the oxyanions of As, Mo, and Cr. Moreover, under circumneutral to slightly alkaline and excess Ca conditions, the speciation of U shifts from uranyl and uranyl sulfate to be dominated by zero-valent or negatively charged uranyl calcium carbonate and uranyl carbonate complexes ($Ca_2UO_2(CO_3)_3$, $UO_2(CO3)_2^{4-}$; Fig. S4†), which are highly stable and mobile and less favorable to undergo sorption onto Fe hydroxides.[81] Anionic Th species under acidic conditions (Fig. S4†) can be strongly retained by sorption onto organic matter as well as Fe mineral precipitates (*e.g.*, schwertmannite, a poorly crystalline Fe oxyhydroxysulfate)[54,61] but as the pH and dissolved carbonate increase in the pond water, the solubility of Th can be enhanced by forming more soluble thorium hydroxide and carbonate complexes (Fig. S4†). Therefore, if liming is to be used to mitigate water and soil acidity at the Taraldrud site, the enhancement of radionuclide mobility due to an alteration of the aqueous speciation should be taken into consideration in the environmental impact assessment as the pond is connected to a stream leading to a drinking water source.

5. Conclusions

The environmental impact of acid-forming alum shale waste rock was studied at a legacy site in Norway. The Taraldrud site can be considered a multiple stressor site, where the mobility of elements is complex as many different solution and solid phase processes occur either simultaneously or separately depending on the prevailing environmental conditions. In general, the distribution of elements within the studied soils exhibited significant heterogeneity, even within small geographical areas, which is probably due to the topography and/or applied remediation strategies (such as the addition of inert filling masses) that have affected the groundwater and drainage flow patterns and hence causing accumulation of contaminants within specific "pockets" of the soil profile. Moreover, the newly formed secondary Fe phases play a key role serving as transient storage locations for dissolved metals, metalloids, and sulfates produce during the on-going weathering of the Taraldrud alum shale waste rock. This retention process is especially true for U which was found in high concentrations within the mixing zone soils, whereas the concentrations in the stream water stayed at background level. Nevertheless, the system is dynamic, and the remobilization of potentially toxic elements needs to be considered when remediation strategies are planned. Neutralization by liming has been allegedly used to treat the ARD leachates at the Taraldrud site, and still the pH in the precipitation pond has been consistently decreasing over a 4 years period, suggesting that this measure has not been sufficient to control the environmental pH. Furthermore, the use of liming may also lead to remobilization of retained contaminants, such as U and Th through carbonate complexation under near-neutral to alkaline pH conditions.

Overall, this study highlights the potential environmental impact of ARD generated from Cambrian–Ordovician alum shale waste rock under the sub-boreal conditions of the Nordic region. The on-going ARD at the Taraldrud site poses environmental and radiological risks to the surrounding ecosystem as the subsurface is affected by mobile and bioavailable species of potentially toxic elements and naturally occurring radionuclides, many exceeding the drinking water guidelines (*i.e.*, Ni, Mn, As, U). Thus further work should focus on studying the stability of formed secondary Fe phases that can affect the long-term fate of the leachable elements in these environments and the formation of neutral rock drainage should be considered if non-acid-forming shale is left at the site after remediation. This work contributes to a better understanding of the environmental impact of acid-forming alum shale waste rock and, consequently, might help with designing better monitoring and managing strategies for multiple stressor sites where the formation of ARD is the major environmental concern.

Data availability

The data supporting this article have been included as part of the ESI.†

Author contributions

Mila K. Pelkonen: conceptualization, methodology, validation, formal analysis, investigation, writing – original draft, writing – review & editing, visualization; Estela Reinoso-Maset: formal analysis, visualization, supervision, writing – original draft, writing – review & editing; Gareth T. W. Law: supervision, writing – review & editing; Ole Christian Lind: supervision, writing – review & editing; Lindis Skipperud: funding acquisition, project administration, supervision.

Conflicts of interest

The authors declare no conflicts of interest in this study.

Acknowledgements

This study has been funded by the Norwegian Research Council through its Centre of Excellence (CoE) funding scheme (Project 223268/F50) and by RadoNorm a Euratom research and training programme 2019–2020 under grant agreement no. 900009 through Norwegian Research Council Project 313070. Synchrotron radiation X-ray powder diffraction data were collected at the Paul Scherrer Institute, Swiss Light Source by Stenman Minerals Ab (**https://stenmanminerals.fi/?lang=en**). We thank the Radiation and Nuclear Safety Authority in Finland (STUK) for performing the gamma spectrometry measurements, and Karl Andreas Jensen and Valeriia Morozova from MINA/NMBU for assistance during ICP-MS/MS measurements.

References

1 A. Akcil and S. Koldas, Acid Mine Drainage (AMD): causes, treatment and case studies, *J. Clean. Prod.*, 2006, **14**, 1139–1145.

2 B. J. Baker and J. F. Banfield, Microbial communities in acid mine drainage, *FEMS Microbiol. Ecol.*, 2003, **44**, 139–152.
3 V. Masindi and K. Muedi, L., in *Environmental Contamination by Heavy Metals*, Heavy Metals, ed. M. S. Hosam El-Din and F. A. Refaat, Rijeka: IntechOpen, 2018, ch. 7, DOI: 10.5772/intechopen.76082.
4 C. Carbone, E. Dinelli, P. Marescotti, G. Gasparotto and G. Lucchetti, The role of AMD secondary minerals in controlling environmental pollution: Indications from bulk leaching tests, *J. Geochem. Explor.*, 2013, **132**, 188–200.
5 K. Åhlgren, V. Sjöberg, B. Allard and M. Bäckström, Groundwater chemistry affected by trace elements (As, Mo, Ni, U and V) from a burning alum shale waste deposit, Kvarntorp, Sweden, *Environ. Sci. Pollut. Res.*, 2021, **28**, 30219–30241.
6 B. Buchardt, A. T. Nielsen and N. G. Schovsbo, Alun Skiferen i Skandinavien, *Norw. J. Geol.*, 1997, **3**, 1–30.
7 IAEA, *The Environmental Behaviour of Radium: Revised Ed.*, International Atomic Energy Agency, 2014.
8 A. Andersson, B. Dahlman, D. G. Gee and S. Snäll, *The Scandinavian Alum Shales*, Uppsala, 1985.
9 A. Elghali, M. Benzaazoua, Y. Taha, H. Amar, Y. Ait-khouia, H. Bouzahzah and R. Hakkou, Prediction of acid mine drainage: Where we are, *Earth Sci. Rev.*, 2023, **241**, 104421.
10 H.-T. Chon, C.-H. Cho, K.-W. Kim and H.-S. Moon, The occurrence and dispersion of potentially toxic elements in areas covered with black shales and slates in Korea, *Appl. Geochem.*, 1996, **11**, 69–76.
11 K. Loukola-Ruskeeniemi, A. Uutela, M. Tenhola and T. Paukola, Environmental impact of metalliferous black shales at Talvivaara in Finland, with indication of lake acidification 9000 years ago, *J. Geochem. Explor.*, 1998, **64**, 395–407.
12 A. Parviainen and K. Loukola-Ruskeeniemi, Environmental impact of mineralised black shales, *Earth-Sci. Rev.*, 2019, **192**, 65–90.
13 F. M. Waersted, P. J. Riss and L. Skipperud, The effect of water exchange on the leaching of alum shale, *Appl. Geochem.*, 2020, **119**, 104610.
14 F. M. Waersted, E. Reinoso-Maset, B. Salbu and L. Skipperud, Limited access to oxygen reduces the release of harmful trace elements from submerged alum shale debris, *Sci. Total Environ.*, 2023, **880**, 163035.
15 N. C. Woo, M. J. Choi and K. S. Lee, Assessment of Groundwater Quality and Contamination from Uranium-Bearing Black Shale in Goesan–Boeun Areas, Korea, *Environ. Geochem. Health*, 2002, **24**, 264–273.
16 C. Oftedahl, On the sulphides of the alum shale in Oslo, *Norw. J. Geol.*, 1955, **35**, 117–120.
17 T. Pabst, E. Sørmo and E. Endre, Geochemical characterisation of Norwegian Cambro-Ordovician black mudrocks for building and construction use, *Bull. Eng. Geol. Environ.*, 2017, **76**, 1577–1592.
18 NGI, *Taraldrud-Grunnforurensning Svartskifer – Supplerende Rapport Til Dokument 125868-RIGM-RAP-003*, Report 20160766-02-R, Norges Geotekniske Institutt, 2017.
19 NRPA, *Radioecology as a Support to Regulatory Decision Making on NORM and Other Legacies, Related Waste Management and Disposal*, Report of an International Workshop, Statens strålevern (NRPA), 2018.
20 QGis, *QGIS Geographic Information System*, Open Source Geospatial Foundation Project, 3.28.15-Firenze, 2022, https://qgis.org/.
21 Kartverket, *Topografisk norgeskart*, https://openwms.statkart.no/skwms1/wms.topo?service=wms&request=getcapabilities, accessed 06.04.2024.
22 NGI, *E6 Taraldrud Alunskifer Tiltaksplan: Supplerende Grunnundersøkelser*, 2021.
23 B. Salbu, Speciation of radionuclides in the environment, in *Encyclopedia of Analytical Chemistry*, ed. R. A. Meyers, John Wiley & Sons Ltd, 2000, pp. 12993–13016.
24 T. Ø. Krogstad, A., *Øvelser I Jordanalyser, NLH: Institutt for Jordfag*, 1987.
25 E. Reinoso-Maset, J. Brown, M. N. Pettersen, F. Steenhuisen, A. Tetteh, T. Wada, T. G. Hinton, B. Salbu and O. C. Lind, Linking heterogeneous distribution of radiocaesium in soils and pond sediments in the Fukushima Daiichi exclusion zone to mobility and potential bioavailability, *J. Environ. Radioact.*, 2020, **211**, 106080.
26 USDA, *Soil Survey Manual – Soil Survey Division Staff; Soil Conservation Service Volume Handbook*, U.S. Department of Agriculture, 2017.
27 Y. P. Kalra, Determination of pH of soils by different methods : collaborative study, *J. AOAC Int.*, 1995, **78**, 310–324.
28 L. P. van Reeuwijk, *Procedures for Soil Analysis*, Technical Paper/International Soil Reference and Information Centre, Wageningen, Netherlands, 6th edn, 2002.
29 H. Tuovinen, D. Vesterbacka, E. Pohjolainen, D. Read, D. Solatie and J. Lehto, A comparison of analytical methods for determining uranium and thorium in ores and mill tailings, *J. Geochem. Explor.*, 2015, **148**, 174–180.
30 F. M. Waersted, K. A. Jensen, E. Reinoso-Maset and L. Skipperud, High Throughput, Direct Determination of 226Ra in Water and Digested Geological Samples, *Anal. Chem.*, 2018, **90**, 12246–12252.
31 H. Tuovinen, M. Pelkonen, J. Lempinen, E. Pohjolainen, D. Read, D. Solatie and J. Lehto, Behaviour of Metals during Bioheap Leaching at the Talvivaara Mine, Finland, *Geosciences*, 2018, **8**, 66.
32 A. Zahra, M. Z. Hashmi, R. N. Malik and Z. Ahmed, Enrichment and geo-accumulation of heavy metals and risk assessment of sediments of the Kurang Nallah—Feeding tributary of the Rawal Lake Reservoir, Pakistan, *Sci. Total Environ.*, 2014, **470–471**, 925–933.
33 M. Barbieri, The Importance of Enrichment Factor (EF) and Geoaccumulation Index (Igeo) to Evaluate the Soil Contamination, *J. Geol. Geophys.*, 2016, **5**, 237.
34 S. Meland, R. Borgstrøm, L. S. Heier, B. O. Rosseland, O. Lindholm and B. Salbu, Chemical and ecological effects of contaminated tunnel wash water runoff to a small Norwegian stream, *Sci. Total Environ.*, 2010, **408**, 4107–4117.

35 C. R. Bern, K. Walton-Day and D. L. Naftz, Improved enrichment factor calculations through principal component analysis: Examples from soils near breccia pipe uranium mines, Arizona, USA, *Environ. Pollut.*, 2019, **248**, 90–100.

36 IAEA, *Handbook of Parameter Values for the Prediction of Radionuclide Transfer in Terrestrial and Freshwater Environments*, International Atomic Energy Agency, Vienna, 2010.

37 J. E. Brown, B. Alfonso, R. Avila, N. A. Beresford, D. Copplestone, G. Pröhl and A. Ulanovsky, The ERICA Tool, *J. Environ. Radioact.*, 2008, **99**, 1371–1383.

38 R Core Team, *R: A Language and Environment for Statistical Computing*, R Foundation for Statistical Computing, Vienna, Austria, 2023, **https://www.R-project.org/**.

39 A. Kassambara and F. Mundt, *Factoextra: Extract and Visualize the Results of Multivariate Data Analyses (R Package Version 1.0.7)*, 2020, **https://CRAN.R-project.org/package=factoextra**.

40 T. Wei and V. Simko, *R Package 'corrplot': Visualization of a Correlation Matrix (Version 0.92)*, 2021, **https://github.com/taiyun/corrplot**.

41 D. Murdoch and D. Adler, *Rgl: 3D Visualization Using OpenGL (R Package Version 1.2.1)*, 2023, **https://CRAN.R-project.org/package=rgl**.

42 D. L. Parkhurst and C. A. J. Appelo, *Description of Input and Examples for PHREEQC Version 3—A Computer Program for Speciation, Batch-Reaction, One-Dimensional Transport, and Inverse Geochemical Calculations*, U.S. Geological Survey Techniques and Methods, 2013, book 6, ch. A43, p. 497, version 3.7.3., **http://pubs.usgs.gov/tm/06/a43/**.

43 S. Y. Lee, Y. Kim, S. A. Kang, B. Chang, H. Hur and Y. J. Lee, Characterization of arsenic (III and V) adsorption on natural schwertmannite formed in acid coal mine drainage: Batch studies and spectroscopic observations, *J. Environ. Chem. Eng.*, 2023, **11**, 109170.

44 S. Rose and W. C. Elliott, The effects of pH regulation upon the release of sulfate from ferric precipitates formed in acid mine drainage, *Appl. Geochem.*, 2000, **15**, 27–34.

45 B. G. Lottermoser, *Mine Wastes: Characterization, Treatment and Environmental Impacts*, Springer, Berlin, 3rd edn, 2010.

46 H. Falk, U. Lavergren and B. Bergbäck, Metal mobility in alum shale from Öland, Sweden, *J. Geochem. Explor.*, 2006, **90**, 157–165.

47 Z. Yuan, X. Ma, S. Wang, L. Yu, P. Zhang, J. Lin and Y. Jia, Effect of co-existent Al(III) in As-rich Acid Mine Drainage (AMD) on As removal during Fe(II) and As(III) abiotic oxidation process, *J. Water Proc. Eng.*, 2021, **44**, 102395.

48 R. Liu, E. B. Altschul, R. S. Hedin, D. V. Nakles and D. A. Dzombak, Sequestration Enhancement of Metals in Soils by Addition of Iron Oxides Recovered from Coal Mine Drainage Sites, *Soil Sediment Contam.: Int. J.*, 2014, **23**, 374–388.

49 N. Unceta, F. Séby, J. Malherbe and O. F. X. Donard, Chromium speciation in solid matrices and regulation: a review, *Anal. Bioanal. Chem.*, 2010, **397**, 1097–1111.

50 E. Markelova, R.-M. Couture, C. T. Parsons, I. Markelov, B. Madé, P. V. Cappellen and L. Charlet, Speciation dynamics of oxyanion contaminants (As, Sb, Cr) in argillaceous suspensions during oxic-anoxic cycles, *Appl. Geochem.*, 2018, **91**, 75–88.

51 D. M. Akob, T. Bohu, A. Beyer, F. Schäffner, M. Händel, C. A. Johnson, D. Merten, G. Büchel, K. U. Totsche and K. Küsel, Identification of Mn(II)-Oxidizing Bacteria from a Low-pH Contaminated Former Uranium Mine, *Appl. Environ. Microbiol.*, 2014, **80**, 5086–5097.

52 M. B. McBride, *Environmental Chemistry of Soils*, Oxford University Press, Oxford, 1994.

53 B. Vriens, E. K. Skierszkan, M. St-Arnault, K. Salzsauler, C. Aranda, K. U. Mayer and R. D. Beckie, Mobilization of Metal(oid) Oxyanions through Circumneutral Mine Waste-Rock Drainage, *ACS Omega*, 2019, **4**, 10205–10215.

54 E. Santofimia, F. J. González, B. Rincón-Tomás, E. López-Pamo, E. Marino, J. Reyes and E. Bellido, The mobility of thorium, uranium and rare earth elements from Mid Ordovician black shales to acid waters and its removal by goethite and schwertmannite, *Chemosphere*, 2022, **307**, 135907.

55 J. Lehto and X. Hou, *Chemistry and Analysis of Radionuclides – Laboratory Techniques and Methodology*, WILEY-VCH Verlag & Co. KGaA, Boschstr, Germany, 2011, vol. 12, p. 69469.

56 S. A. Cumberland, G. Douglas, K. Grice and J. W. Moreau, Uranium mobility in organic matter-rich sediments: A review of geological and geochemical processes, *Earth-Sci. Rev.*, 2016, **159**, 160–185.

57 W. R. Bower, K. Morris, F. R. Livens, J. F. W. Mosselmans, C. M. Fallon, A. J. Fuller, L. Natrajan, C. Boothman, J. R. Lloyd, S. Utsunomiya, D. Grolimund, D. Ferreira Sanchez, T. Jilbert, J. Parker, T. S. Neill and G. T. W. Law, Metaschoepite Dissolution in Sediment Column Systems-Implications for Uranium Speciation and Transport, *Environ. Sci. Technol.*, 2019, **53**, 9915–9925.

58 M. C. Duff, J. U. Coughlin and D. B. Hunter, Uranium co-precipitation with iron oxide minerals, *Geochim. Cosmochim. Acta*, 2002, **66**, 3533–3547.

59 A. J. Fuller, P. Leary, N. D. Gray, H. S. Davies, J. F. W. Mosselmans, F. Cox, C. H. Robinson, J. K. Pittman, C. M. McCann, M. Muir, M. C. Graham, S. Utsunomiya, W. R. Bower, K. Morris, S. Shaw, P. Bots, F. R. Livens and G. T. W. Law, Organic complexation of U(VI) in reducing soils at a natural analogue site: Implications for uranium transport, *Chemosphere*, 2020, **254**, 126859.

60 N. R. E. N. Impens, K. A. Jensen, L. Skipperud, A. V. Gompel and N. Vanhoudt, In-depth understanding of local soil chemistry reveals that addition of Ca may counteract the mobilisation of 226Ra and other pollutants before wetland creation on the Grote Nete river banks, *Sci. Total Environ.*, 2022, **823**, 153703.

61 Z. U. W. Mahmood and C. A. R. Mohamed, Thorium, in *Radionuclides in the Environment*, ed. D. A. Atwood, 2010, p. 544.

62 H. Gautneb and O. M. Sæther, *A Compilation of Previously Published Geochemical Data on the Lower Cambro-Silurian*

Sedimentary Sequence, Including the Alum Shales in the Oslo region, (Report 2009.053), Geological Survey of Norway, 2009.

63 Klima- og miljødepartementet, *Forskrift Om Radioaktiv Forurensning Og Avfall*, 2011, Report FOR-2010-11-01-1394, **https://lovdata.no/dokument/SF/forskrift/2010-11-01-1394**.

64 UNSCEAR, Sources and Effects of Ionizing Radiation, Report to the General Assembly with Scientific Annexes, *United Nations Scientific Committee on Effects of Atomic Radiation*, United Nations, 2008.

65 WHO, *Guidelines for Drinking water quality*, **https://www.who.int/publications/i/item/9789241549950**, accessed 06.04.2024.

66 IAEA, *The Environmental Behavior of Uranium - Technical Reports Series No. 488*, International Atomic Energy Agency, Vienna, 2023.

67 E. Dudel, C. Brackhage, H. Dienemann, M. Mkandawire and A. Weiske, presented in part at the - Title, Capacity of natural attenuation of trace contaminants from uranium mine tailing waters in nature-like constructed wetlands, *Mine Water 2004*, University of Newcastle, 2004.

68 J. M. Popic, D. H. Oughton, B. Salbu and L. Skipperud, Transfer of naturally occurring radionuclides from soil to wild forest flora in an area with enhanced legacy and natural radioactivity in Norway, *Environ. Sci.: Processes Impacts*, 2020, **22**, 350–363.

69 P. Roivainen, S. Makkonen, T. Holopainen and J. Juutilainen, Transfer of elements relevant to radioactive waste from soil to five boreal plant species, *Chemosphere*, 2011, **83**, 385–390.

70 E. Reinoso-Maset and J. Ly, Study of uranium(VI) and radium(II) sorption at trace level on kaolinite using a multisite ion exchange model, *J. Environ. Radioact.*, 2016, **157**, 136–148.

71 E. Reinoso-Maset, P. J. Worsfold and M. J. Keith-Roach, The effect of EDTA, NTA and picolinic acid on Th(IV) mobility in a ternary system with natural sand, *Environ. Pollut.*, 2012, **162**, 399–405.

72 E. Reinoso-Maset, P. J. Worsfold and M. J. Keith-Roach, Effect of organic complexing agents on the interactions of Cs+, Sr2+ and UO22+ with silica and natural sand, *Chemosphere*, 2013, **91**, 948–954.

73 H. Vandenhove, M. Van Hees, J. Wannijn, K. Wouters and L. Wang, Can we predict uranium bioavailability based on soil parameters? Part 2: soil solution uranium concentration is not a good bioavailability index, *Environ. Pollut.*, 2007, **145**, 577–586.

74 J. M. Popic, B. Salbu, T. Strand and L. Skipperud, Assessment of radionuclide and metal contamination in a thorium rich area in Norway, *J. Environ. Monit.*, 2011, **13**, 1730–1738.

75 D. H. Oughton, G. Strømman and B. Salbu, Ecological risk assessment of Central Asian mining sites: application of the ERICA assessment tool, *J. Environ. Radioact.*, 2013, **123**, 90–98.

76 L. Skipperud, E. Alvarenga, O. C. Lind, H.-C. Teien, K. E. Tollefsen, B. Salbu and F. M. Wærsted, Construction works in areas with sulphide containing rock, *Case: Effects and Environmental Risks Related to Alum Shale Disposal Site (651)*, Norwegian Public Roads Administration, 2016.

77 NIVA, *Riverine Inputs and Direct Discharges to Norwegian Coastal Waters - 2016*, Norwegian Institute for Water Research (NIVA), 2017.

78 B. Salbu, Radionuclides Speciation, in *Encyclopedia of Inorganic and Bioinorganic Chemistry*, ed. R. A. Scott, 2011, DOI: **10.1002/9781119951438.eibc04122011**.

79 S. Rognerud and E. Fjeld, Trace Element Contamination of Norwegian Lake Sediments, *AMBIO A J. Hum. Environ.*, 2001, **30**, 11–19.

80 S. Grangeon, C. Roux, C. Lerouge, P. Chardon, R. Beuzeval, G. Montavon, F. Claret and T. Grangeon, Geochemical and mineralogical characterization of streams and wetlands downstream a former uranium mine (Rophin, France), *Appl. Geochem.*, 2023, **150**, 105586.

81 B. D. Stewart, M. A. Mayes and S. Fendorf, Impact of Uranyl–Calcium–Carbonato Complexes on Uranium(VI) Adsorption to Synthetic and Natural Sediments, *Environ. Sci. Technol.*, 2010, **44**, 928–934.